NONLINEAR STATIC AND DYNAMIC ANALYSIS OF BEAM STRUCTURES USING FULLY INTRINSIC EQUATIONS

A Dissertation
Presented to
The Academic Faculty

by

Zahra Sotoudeh

In Partial Fulfillment
of the Requirements for the Degree
Doctor of Philosophy in the
School of Aerospace Engineering

Georgia Institute of Technology
August 2011

NONLINEAR STATIC AND DYNAMIC ANALYSIS OF BEAM STRUCTURES USING FULLY INTRINSIC EQUATIONS

Approved by:

Prof. Dewey H. Hodges, Advisor
School of Aerospace Engineering
Georgia Institute of Technology

Prof. Olivier A. Bauchau
School of Aerospace Engineering
Georgia Institute of Technology

Prof. Massimo Ruzzene
School of Aerospace Engineering
Georgia Institute of Technology

Prof. Michael Leamy
School of Mechanical Engineering
Georgia Institute of Technology

Prof. Arash Yavari
School of Civil Engineering
Georgia Institute of Technology

Date Approved: 30 June 2011

To my mom and dad

ACKNOWLEDGEMENTS

It is a pleasure to thank many individuals who made this dissertation possible. I would like to start with my adviser Prof. Dewey Hodges. I could not imagine or hope for a better academic advisor. I learned many things during and before my years of working with him, and I am sure I will continue to learn from him in years to come. He generously helped me during my M.S. degree before I joined his research group at Georgia Tech. He gave me freedom in my research, so I could learn how to think and come up with new ideas; on the other hand, he gave me advice to keep me on track towards graduation. He truly touched my life in so many levels.

I would like to sincerely thank Prof. David Peters. He helped me way before I joined Georgia Tech. He generously spent hours and hours of his valuable time teaching me about dynamic inflow theory. He is the type of researcher and professor I look to as a role model. I also need to thank Prof. Eral Dowell for introducing me to Profs. Hodges and Peters for the first time.

I would like to thank Prof. Oliver Bauchau. He is the best teacher I can imagine. His teaching method is fantastic; I enjoyed being in many of his classes. I can never ever forget the first few sessions of Structural Analysis class. I could not believe that what I saw is real and not a dream. His office door is always open and he is always there with a big smile and unlimited time to listen and answer.

When it comes to teaching I also should thank Prof. Wassim Haddad. He is the most passionate teacher I have ever had. Unfortunately I discovered him late in my PhD studies. Had I been in his class earlier in my studies, there would have been a great chance that this thesis would be in control area instead of structural dynamics. His office door is always open to students and he is always one email away.

I also would like to thank Prof. Marilyn Smith for her wonderful class. She is the type of female professor who pursues research in a hardcore engineering field. I always look up

to her as a role model. I had the honor to work for her in Summer 2011. She is the most understanding boss one can hope for.

I would like to thank Prof. Vigor Yang for his leadership in the School of Aerospace Engineering and his continuous support. I also would like to thank Profs. Jeff Jagoda, George Kardomateas, Lakshmi Sankar, Karen Feigh, Wenbin Yu and Dr. Karen Head for their support and encouragement.

This work is largely based on the research of Prof. Mayuresh J. Patil and Dr. Chongseok Chang. Both kindly helped me to speed up in my studies and provided me with computer programs. I gratefully appreciated technical discussions with both. I also would like to thank Dr. Chongseok Chang for his friendship and mentorship during my PhD studies.

A requirement for the PhD degree in Aerospace Engineering at Georgia Tech is that the work of the student must be evaluated and approved by a thesis committee, so I am thankful to all five members of my committee for serving this important duty. Profs. Dewey Hodges, Olivier Bauchau and Massimo Ruzzene have been on my committee since my proposal. Profs. Michael Leamy and Arash Yavari joined the committee to evaluate this thesis and my defense presentation.

Having financial support is a measurement of value of any research work. I am fortunate to have been financially supported for my entire studies at Georgia Tech, so I am grateful to my sponsors. My work on joined-wing aircraft was supported by NASA Dryden. Development of BAAR was supported by Bell Helicopter Textron. I also would like to thank Dr. Mark Wasikowsi for his technical support. The assistance of Mr. Jeffrey Bosworth in setting up some DYMORE cases is gratefully acknowledged.

During my years of studies at Georgia Tech I enjoyed friendship of many of Aerospace students. I will provide only a short list. I would like to thank Dr. Jimmy Ho for his friendship in addition to many useful technical discussions. I highly appreciate his effort to uphold the Georgia Tech honor code. I also like to thank soon-to-be Drs. Catherine Phan and Akash Dixit for their friendship, many useful technical discussions and their support during my academic presentations. I also would like to thank soon-to-be Dr. Yannick Van Weddingen for friendship and being a kind and encouraging officemate. I should thank

him for useful technical and nontechnical discussions, and most importantly for providing me with a continuous supply of chocolate. I also need to thank Dr. Samer Tawfik for his friendship, very useful technical discussions and a continuous flow of snacks.

Last but the most importantly, I would like to thank my mom and dad for their extraordinary support. They have always trusted me and truly love me for who I am. Not that the contents of this thesis is perfect, but all my accomplishments in life would have been impossible without their unconditional love and support.

TABLE OF CONTENTS

LIST OF TABLES

LIST OF FIGURES

Nomenclature

General Nomenclature

b	Undeformed beam cross-sectional frame of reference
B	Deformed beam cross-sectional frame of reference
$\mathbf{b}_i$	Unit vector in undeformed beam cross-sectional frame of reference, $(i = 1, 2, 3)$
$\mathbf{B}_i$	Unit vector in deformed beam cross-sectional frame of reference, $(i = 1, 2, 3)$
C^{AB}	Transformation matrix from B frame of reference to A
e_1	Column matrix $\lfloor 1 \;\; 0 \;\; 0 \rfloor^T$
f	Column matrix of distributed applied force measures in $\mathbf{B}_i$ basis
F	Column matrix of internal force measures in $\mathbf{B}_i$ basis
H	Column matrix of cross-sectional angular momentum measures in $\mathbf{B}_i$ basis
i	Inertial frame of reference
$\mathbf{i}_i$	Unit vectors for inertial frame of reference $(i = 1, 2, 3)$
I	Cross-sectional inertia matrix
k	Column matrix of initial curvature and twist measures in $\mathbf{b}_i$ basis
K	Column matrix of deformed beam curvature measures in $\mathbf{B}_i$ basis
m	Column matrix of distributed applied moment measures in $\mathbf{B}_i$ basis
M	Column matrix of internal moment measures in $\mathbf{B}_i$ basis
P	Column matrix of cross-sectional linear momentum measures in $\mathbf{B}_i$ basis
r	Column matrix of position vector measures in $\mathbf{b}_i$ basis
u	Column matrix of displacement vector measures in $\mathbf{b}_i$ basis
V	Column matrix of velocity measures in $\mathbf{B}_i$ basis
x_1	Axial coordinate of beam
Δ	Identity matrix
γ	Column matrix of extensional and shear measures (1D generalized force strain measures)
κ	Column matrix of elastic twist and curvature measures (1D generalized moment strain measures)
μ	Mass per unit length

ξ Offset of center of mass from origin of frame of reference in $\mathbf{b}_i$ basis

Ω Column matrix of cross-sectional angular velocity measures in $\mathbf{B}_i$ basis

$(\,)'$ Partial derivative of $(\,)$ with respect to x_1

$\dot{(\,)}$ Partial derivative of $(\,)$ with respect to time

Chapter 4

a Deformed beam aerodynamic frame of reference

C_a Short for C^{Ba}, the direction cosine matrix of frame B with respect to frame a

e_1 Column matrix $\lfloor 1 \;\; 0 \;\; 0 \rfloor^T$

e_2 Column matrix $\lfloor 0 \;\; 1 \;\; 0 \rfloor^T$

e_3 Column matrix $\lfloor 0 \;\; 0 \;\; 1 \rfloor^T$

EA Extensional stiffness for isotropic beam

EI_α Bending stiffness for isotropic beam about x_α $(\alpha = 2, 3)$

g Gravitational constant

GJ Torsional stiffness for isotropic beam

y_{ac} Offset of aerodynamic center from the beam reference line along $\mathbf{b}_2$

Chapter 5

$\mathbf{A}_i$ Unit vectors of frame A, $(i = 1, 2, 3)$

$\mathbf{U}$ Inboard bearing displacement vector

u Column matrix of displacement vector measures in $\mathbf{b}_i$ basis

$\mathbf{V}$ Velocity vector

V Column matrix of velocity measures in $\mathbf{B}_i$ basis

x_1 Axial coordinate of beam

$\mathbf{\Theta}$ Inboard bearing rotational parameters

$(\,)_m$ Index; can be 1,2,3

$(\,)_n$ Index; can be 1,2,3

$( )_q$ Index; can be 1,2,3

SUMMARY

Beams are structural members with one dimension much larger than the other two. Examples of beams include propeller blades, helicopter rotor blades, and high aspect-ratio aircraft wings in aerospace engineering; shafts and wind turbine blades in mechanical engineering; towers, highways and bridges in civil engineering; and DNA modeling in biomedical engineering. Beam analysis includes two sets of equations: a generally linear two-dimensional problem over the cross-sectional plane and a nonlinear, global one-dimensional analysis.

This research work deals with a relatively new set of equations for one-dimensional beam analysis, namely the so-called fully intrinsic equations. Fully intrinsic equations comprise a set of geometrically exact, nonlinear, first-order partial differential equations that is suitable for analyzing initially curved and twisted anisotropic beams. A fully intrinsic formulation is devoid of displacement and rotation variables, making it especially attractive because of the absence of singularities, infinite-degree nonlinearities, and other undesirable features associated with finite rotation variables.

In spite of the advantages of these equations, using them with certain boundary conditions presents significant challenges. This research work will take a broad look at these challenges of modeling various boundary conditions when using the fully intrinsic equations. Hopefully it will clear the path for wider and easier use of the fully intrinsic equations in future research.

This work also includes application of fully intrinsic equations in structural analysis of joined-wing aircraft, different rotor blade configuration and LCO analysis of HALE aircraft.

CHAPTER I

INTRODUCTION AND LITERATURE REVIEW

Beams are structural members with one dimension much larger than the other two. Examples of beams include propeller blades, helicopter rotor blades, and high aspect-ratio aircraft wings in aerospace engineering; shafts and wind turbine blades in mechanical engineering; towers, highways and bridges in civil engineering [34]; and DNA and vein modeling in biomedical engineering. Beam analysis includes two sets of equations: a generally linear two-dimensional problem over the cross-sectional plane [20, 5, 65, 32] and a nonlinear, global one-dimensional analysis. An extensive literature survey of the modern history of beam analysis can be found in Ref. [32].

This work deals with a relatively new set of equations for one-dimensional beam analysis, namely the so-called fully intrinsic equations [31]. Fully intrinsic equations comprise a set of geometrically exact, nonlinear, first-order partial differential equations that is suitable for analyzing initially curved and twisted anisotropic beams. A fully intrinsic formulation is devoid of displacement and rotation variables, making it especially attractive because of the absence of singularities, infinite-degree nonlinearities, and other undesirable features associated with finite rotation variables.

Ref. [33] presents a wide literature review of the fully intrinsic equations. The concept of fully intrinsic equations for dynamics of beams goes back over 25 years before the publication of Ref. [31], at least back to the work of Hegemier and Nair [24]. However, the equations of Ref. [31] appear to be unique in that (a) they constitute a geometrically exact, fully intrinsic, dynamic formulation including initial curvature and twist, shear deformation, rotary inertia, and general anisotropy and (b) their use is explicitly suggested for a dynamic formulation without their being augmented with some form of angular displacement variables, such as orientation angles, Rodrigues parameters, or the like used in mixed formulations [25].

Fully intrinsic formulations have been used to study the static equilibrium behavior of

statically determinate beams [40] and the dynamics of cables and DNA molecules [22]. These equations have been applied to the aeroelastic analysis of HALE aircraft in the computer code NATASHA (Nonlinear Aeroelastic Trim and Stability Analysis of HALE Aircraft) [44, 11, 60]. They were also applied to the modeling helicopter rotor blades [46, 19] and to the simulation of ground vibration testing of HALE aircraft [8]. Finally, and most recently, detailed studies of the free-vibration [10] and stability [9] of curved beams were presented using fully intrinsic equations.

The rest of this chapter presents a discussion of the motivations for this work, a brief literature review on joined-wing aircraft, and helicopter rotor blades (two different applications of fully intrinsic equations which are addressed in this work). In Chapter 2 the fully intrinsic equations are briefly introduced. Chapter 3 is devoted to some general insight of using fully intrinsic equations with different boundary conditions. Chapter 4 presents detailed introduction of the incremental method and joined-wing aircraft. Chapter 5 deals with applications to helicopter rotor blade dynamics. Finally, conclusions and future work will be presented in Chapter 6.

1.1 Motivation

In spite of all the advantages of fully intrinsic equations, using them with certain boundary conditions can present some challenges. So far, these equations have been used to model structures with simple boundary conditions [44, 11]. This research will take a broad look at challenges of modeling various boundary conditions when using the fully intrinsic equations. This research hopefully will clear the path for wider and easier use of the fully intrinsic equations in future research. Next, the fully intrinsic equations are applied to more complex structures such as joined-wing aircraft and helicopter rotor blades.

1.2 Joined-wing aircraft

The joined-wing concept, as introduced by Wolkovitch [63], features diamond-shapes in the planform and front views. High-altitude long-endurance (HALE) aircraft usually have high-aspect-ratio wings, resulting in greater flexibility than conventional aircraft. Recently, the joined-wing concept has been revisited as a lighter alternative configuration for HALE

aircraft. The analysis of such aircraft requires the development of nonlinear analysis and special design tools. Due to the unusual topology of joined-wing airplane configurations, the effects of structural deformation on the static aerodynamic and aeroelastic behavior are more difficult to predict. Deformation of the structure at certain locations may produce large changes in angle of attack at other locations of the lifting surfaces. Efforts to minimize structural weight may create aeroelastic instabilities that are not encountered in more conventional aircraft designs. For a joined-wing aircraft, the first sign of failure may be in the buckling of the aft member as the structure is softened. Flutter and divergence may also become problems in these members due to the reduction in natural frequencies as they go into compression. As the aircraft becomes more flexible, the nature of the geometric structural nonlinearities become more important.

Several analyses have been developed to address the unique features of joined-wing aircraft. The oldest appears to be in 1991 [36] in which a parametric study of aerodynamic, structural and geometric properties of joined-wing aircraft is performed. Rather than cite individual works in the 1990s, we here refer to a survey by Livne [39] of works pertaining to joined-wing aircraft and their aeroelastic behavior through 2001.

After 2001, we note works pertaining primarily to structural aspects separately from those that consider aeroelastic phenomena. Primarily structures-oriented studies include Refs. [2, 50], which focus on design of a joined-wing configuration with consideration of different structural and geometric properties. Patil performed a nonlinear structural analysis of a joined-wing using a mixed formulation [43] and compared his results with experimental data [17]. Ref. [37] performs a study on buckling phenomena in joined-wing aircraft. Ref. [23] uses an equivalent static load and beam theory in optimization of joined-wing aircraft. Finally, there are several experimental works on joined-wing aircraft [17, 47, 4] that are primarily structural in nature.

Those analyses and investigations after 2001 that deal with aeroelastic effects begin with Weisshaar and Lee [62] who investigate the effects of joined-wing aircraft geometry, mass distribution and structural design on aeroelastic flutter mechanisms and aircraft weight. They also show how weight, strength and stiffness should be distributed for an effective

design. Their work relied on two different methods: a Rayleigh-Ritz method and the static and dynamic aeroelastic analysis capabilities in ASTROS (Automated STRuctural Optimization System) [62]. Cesnik et al. [7, 6] introduced an approach to effectively model the nonlinear aeroelastic behavior of highly flexible aircraft. The analysis was based on a nonlinear finite element framework in which nonlinear strain measures are the primary variables instead of displacements and rotations. The resulting low-order formulation captures large deflections of the wings along with the unsteady subsonic aerodynamic forces acting on them. An integrated process is presented in Ref. [3] that advances the design of an aeroelastic joined-wing concept by incorporating physics-based results at the system level. For example, this process replaces empirical mass estimation with a high-fidelity analytical mass estimation. Elements of nonlinear structures, aerodynamics, and aeroelastic analyses were incorporated along with vehicle configuration design using a traditional finite element analysis. Ref. [13] focuses on the aeroelastic behavior of joined-wing aircraft with particular attention to the effect of structural nonlinearity on divergence and flutter. Ref. [14] uses a modal reduction method and meanwhile tries to capture nonlinearity effects. Later, using the same method, Demasi et al. [15] performed an aeroelastic analysis of a joined-wing aircraft model. Ref. [16] presented a parametric study on aeroelastic behavior of two types of joined-wing aircraft. Ref. [38] studied a gust response sensitivity analysis for a joined-wing model. Ref. [56] uses an incremental method to revisit some of the parametric studies presented by Ref. [36]. A formulation for a symmetric and balanced maneuvering load alleviation taking into account the aircraft flexibility has been derived in Ref. [41].

1.3 Helicopter rotor blades

As it is shown in chapter 3 fully intrinsic equations are very suitable for modeling rotating beams. This research includes using fully intrinsic equations in dynamic response and eigenvalue analysis. This part of work is sponsored by Bell Helicopter Textron.

Many papers have been published on the general subject of modeling helicopter blade dynamics and aeroelasticity. The literature is so overwhelmingly rich that a comprehensive literature review is clearly not within the scope of this work. Here are only a few examples:

Refs. [28, 26, 64, 66] in structural dynamics of rotor blades and [29, 51, 61, 12] in aeroleastic analysis of helicopter blades and/or rotors. Most approaches to helicopter structural or aeroelastic analysis have made use of some kind of rotational parameters, such as orientation angles or Rodrigues parameters. Using instead the fully intrinsic equations [31] is both convenient and novel, since there is no need for rotational parameters, and the maximum degree of nonlinearity is only two. Ref. [46] and [19] used fully intrinsic equations to study single-load-path bearingless helicopter rotor blades. This work uses the fully intrinsic equations in more complex helicopter rotors, a contribution that is missing in the literature.

CHAPTER II

GENERAL THEORY – FULLY INTRINSIC EQUATIONS

In this chapter the foundation of this thesis is reviewed. The fully intrinsic equations [31] are introduced briefly, as well as typical solution procedures for these equations.

This chapter is mostly adopted from Refs. [44, 57], with the authors' permission.

2.1 Frames of reference

Figure 1 shows a beam in its undeformed and deformed states. At each point along the undeformed beam axis, a frame of reference $b(x_1)$ is introduced; and at each point along the deformed beam axis, a frame of reference $B(x_1, t)$ is introduced. Here are other frames of reference which are used in this work:

1. Inertial frame of reference, i. The unit vector $\mathbf{i}_3$ is in the opposite direction of gravity.

2. Aerodynamic frame of reference, a. Aerodynamic lift and moment are defined in this frame. $\mathbf{a}_2$ and $\mathbf{a}_3$ are defined in the airfoil frame with $\mathbf{a}_3$ pointing perpendicular to the aerodynamic surface.

The fully intrinsic equations contain variables that are expressed in the bases of frames b and B and can be written in compact matrix form as [31]

$$\begin{aligned} F_B' + \widetilde{K}_B F_B + f_B &= \dot{P}_B + \widetilde{\Omega}_B P_B \\ M_B' + \widetilde{K}_B M_B + (\widetilde{e_1} + \widetilde{\gamma})\Omega_B + m_B &= \dot{H}_B + \widetilde{\Omega}_B H_B + \widetilde{V}_B P_B \end{aligned} \tag{1}$$

$$\begin{aligned} V_B' + \widetilde{K}_B V_B + (\widetilde{e_1} + \widetilde{\gamma})\Omega_B &= \dot{\gamma} \\ \Omega_B' + \widetilde{K}_B \Omega_B &= \dot{\kappa} \end{aligned} \tag{2}$$

$$\begin{Bmatrix} \gamma \\ \kappa \end{Bmatrix} = \begin{bmatrix} R & S \\ S^T & T \end{bmatrix} \begin{Bmatrix} F_B \\ M_B \end{Bmatrix} \tag{3}$$

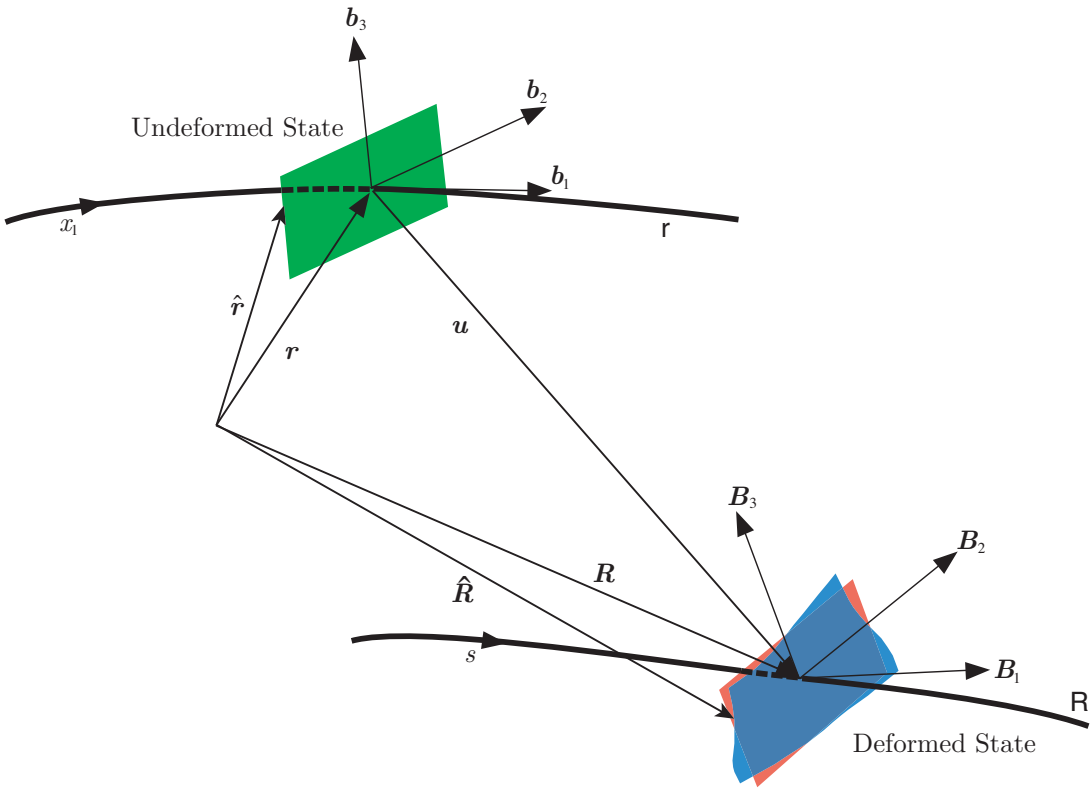

Figure 1: Sketch of beam kinematics

$$\left\{ \begin{array}{c} P_B \\ H_B \end{array} \right\} = \left[\begin{array}{cc} \mu\Delta & -\mu\widetilde{\xi} \\ \mu\widetilde{\xi} & I \end{array} \right] \left\{ \begin{array}{c} V_B \\ \Omega_B \end{array} \right\} \tag{4}$$

Equations (1a) and (1b) are partial differential equations for linear and angular momentum balance, respectively. Equations (2) are kinematical partial differential equations. Equations (3) and (4) are constitutive equations and generalized velocity-momentum equations. This is a complete and closed set of algebraic and first-order partial differential equations. The strain- and velocity-displacement equations are implicit in the intrinsic kinematical partial differential equations [31].

As mentioned before, fully intrinsic equations include neither displacement nor rotation variables. However, displacement at any point and direction cosines for any vector of interest can be calculated either during a simulation or as a post-processing step. For example, the

direction cosines of $\mathbf{b}_i$ and $\mathbf{B}_i$ may be found as

$$\begin{aligned}(C^{bi})' &= -\widetilde{k}C^{bi} \\ (C^{Bi})' &= -(\widetilde{k}+\widetilde{\kappa})C^{Bi}\end{aligned} \tag{5}$$

and the measure numbers of position vectors for the undeformed and deformed beam may be found from

$$\begin{aligned}r_i' &= C^{ib}e_1 \\ (r_i+u_i)' &= C^{iB}(e_1+\gamma)\end{aligned} \tag{6}$$

where the superscript i represents an inertial frame of reference.

2.2 Solution procedure

Equations (1) – (3) comprise a system of algebraic-partial differential equations. Fortunately in case of linear constitutive laws, it is very easy to put the system into the form of partial differential equations by substituting expressions for γ and κ from the algebraic Eqs. (3a) and expressions for P and H from the algebraic Eqs. (3b) into Eqs. (1) and (2). This work deals with the case of linear constitutive laws. In this case, the resulting system of governing equations will consist of 12 partial differential equations, each one of which is first order in x_1 and t; the system thus needs 12 boundary conditions and 12 initial conditions.

One method to solve the partial differential equations is to simultaneously discretize both in time and space [22], leading directly to a time simulation analysis. This approach can be very costly. Common but less general approaches to solving these equations generally consist of two steps: First, find a steady-state solution, and second linearize the governing equations about the steady-state solution. The steady-state solution may or may not be time-dependent. For example, the equations governing a static steady-state solution may be found by dropping all time derivatives and all time-dependent terms. Then, a set of nonlinear algebraic equations can be derived by applying a finite element or finite difference spatial discretization [46]. In the second step, once a steady-state solution is found, one may linearize about it. The resulting homogeneous, linearized, ordinary differential equations may be time-varying, which is often the case in stability analysis of rotating systems. Even in such cases, it is sometimes possible to reduce the solution to that of an eigenvalue problem

without periodic coefficients; for example, in the analysis of multibladed rotors one may do so by employing the method of multi-blade coordinates. When this is possible, it obviates the computationally expensive application of Floquet theory [18]. When the homogeneous, linearized, ordinary differential equations are not time-varying, they can be discretized using a finite element or finite difference spatial discretization, and the resulting linear algebraic equations solved as a generalized eigenvalue problem. This work focuses on those challenges regarding various boundary conditions for steady-state and constant-coefficient eigenvalue problems.

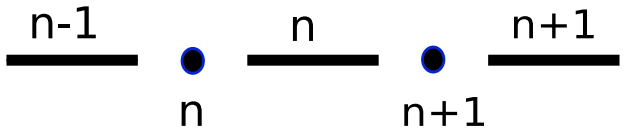

Figure 2: Typical element of a beam

Figure 2 shows a typical discretization of a beam. One may use a simple central differencing for force, moment, velocity and angular velocity or linear shape functions for these variables. A discretized form of the fully intrinsic equations can be written in the form

$$\begin{aligned}
\frac{\widehat{F}_l^{n+1}-\widehat{F}_r^n}{dl}+(\widetilde{\overline{\kappa}}^n+\widetilde{k}^n)\overline{F}^n+\overline{f}^n-\dot{\overline{P}}^n-\widetilde{\overline{\Omega}}^n\overline{P}^n&=0\\
\frac{\widehat{M}_l^{n+1}-\widehat{M}_r^n}{dl}+(\widetilde{\overline{\kappa}}^n+\widetilde{k}^n)\overline{M}^n+(\widetilde{e_1}+\widetilde{\overline{\gamma}}^n)\overline{F}^n+\overline{m}^n-\dot{\overline{H}}^n-\widetilde{\overline{\Omega}}^n\overline{H}^n-\widetilde{\overline{V}}^n\overline{P}^n&=0\\
\frac{\widehat{V}_l^{n+1}-\widehat{V}_r^n}{dl}+(\widetilde{\overline{\kappa}}^n+\widetilde{k}^n)\overline{V}^n+(\widetilde{e_1}+\widetilde{\overline{\gamma}}^n)\overline{\Omega}^n-\dot{\overline{\gamma}}^n&=0\\
\frac{\widehat{\Omega}_l^{n+1}-\widehat{\Omega}_r^n}{dl}+(\widetilde{\overline{\kappa}}^n+\widetilde{k}^n)\overline{\Omega}^n-\dot{\overline{\kappa}}^n&=0
\end{aligned} \tag{7}$$

where $\overline{f}^n$ and $\overline{m}^n$ account for the external forces and moments applied on the n^{th} element. The element variables ($\overline{X}^n$) are secondary variables, which are related to the primary nodal variables as follows:

$$\begin{aligned}
\overline{F}^n&=\frac{\widehat{F}_l^{n+1}+\widehat{F}_r^n}{2}\\
\overline{M}^n&=\frac{\widehat{M}_l^{n+1}+\widehat{M}_r^n}{2}\\
\overline{V}^n&=\frac{\widehat{V}_l^{n+1}+\widehat{V}_r^n}{2}\\
\overline{\Omega}^n&=\frac{\widehat{\Omega}_l^{n+1}+\widehat{\Omega}_r^n}{2}
\end{aligned} \tag{8}$$

Variables are assumed to be different at right and left side of each node, so one can easily account for discontinuity at each node.

The fully intrinsic equations have been used in the computer code NATASHA (Nonlinear Aeroelastic Trim and Stability of HALE Aircraft). The present research includes a wide validation study of NATASHA [60]. Another computer program that falls within the scope of the present research has been developed for Bell Helicopter Textron, BAAR (Bell Aeromechanics Analysis for Rotors).

2.3 Example

In order to illustrate the concept of fully intrinsic equation, the traditional displacement equation of a uniform, isotropic beam is written in the form of fully intrinsic equations. Figure 3 shows an element of a beam in $\boldsymbol{b_2} - \boldsymbol{b_1}$ plane. The following assumptions are used in the most simplest beam theory for this problem.

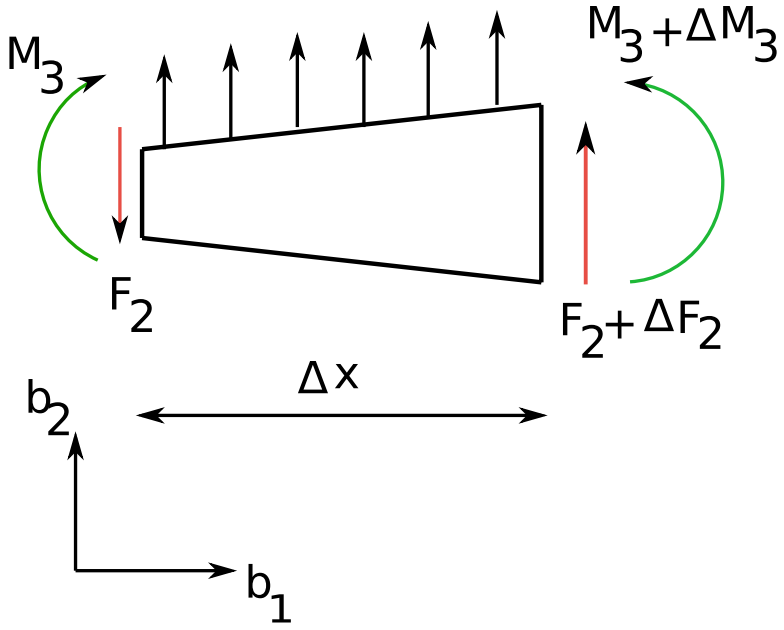

Figure 3: Sketch of an element of a beam

- Euler- Bernoulli beam theory
- Neglecting the effect of rotary inertia
- Isotropic, uniform beam

- Linear theory

Assumption of linear theory means deformed and undeformed configuration assumed to be very close to each other; therefore, the equilibrium equations are written about undeformed state instead of deformed state. The following equation shows the displacement based governing equations of this beam.

$$(EIu'')'' + \mu\ddot{u} = f_2 \tag{9}$$

where u is transverse displacement in b_2 direction, μ is mass per unit of length, f_2 is the transverse distributed load, $(\,)'$ is derivative with respect to x and $\dot{(\,)}$ is derivative with respect to time (t). The derivation of this equation can be found in Ref. [35]. Bending moment is proportional to curvature. One can find this relationship by writing the equilibrium equation over the cross section of the beam. Curvature can be written as

$$\kappa_3 = u'' \tag{10}$$

so

$$EIu'' = M_3 \tag{11}$$

Substituting Eq. (10) in Eq. (11), one will have

$$\kappa_3 = \frac{M_3}{EI} \tag{12}$$

Equation (12) is the simplified form of Eq. (3) for the simple problem at hand. One can also write velocity as time derivative of displacement.

$$\dot{u} = V_2 \tag{13}$$

Therefore

$$\ddot{u} = \dot{V}_2 \tag{14}$$

Substituting Eq. (14) and Eq. (13) into Eq. (9)

$$M_3'' + \mu\dot{V}_2 = f_2 \tag{15}$$

and

$$\mu V_2 = P_2 \tag{16}$$

Equation (16) is the simplified form of Eq. (4). Finally, Eq. (15) is simplified as

$$M_3'' + \dot{P}_2 = f_2 \tag{17}$$

Using the following equilibrium (moment balance) equation, one can write Eq. (17) in first order form.

$$M_3' + F_2 = 0 \tag{18}$$

Substituting Eq. (18) into Eq. (17) one will have

$$F_2' + f_2 = \dot{P}_2 \tag{19}$$

Equations (17) and (18) are the equations of motion for the problem at hand (simplified form of Eq. (1)). One also needs to write strain-displacement equation. In this case strain-displacement equations is Eq. (10). One can write the slope of the beam (θ_3) as u' because of the Euler-Bernoulli assumption. Hence,

$$\dot{\theta}_3 = \Omega_3 \tag{20}$$

Therefore,

$$\dot{\theta}_3' = \Omega_3' = \dot{u}'' = \dot{\kappa}_3 \tag{21}$$

also

$$V_2' = \dot{u}' = \Omega_3 \tag{22}$$

Equations (21) and (22) are the simplified kinematical partial differential equations (Eqs. (2)) for the problem at hand. Finally, the fully intrinsic equations for this simple example

are

$$
\begin{aligned}
&F_2' + f_2 = \dot{P}_2 \\
&M_3' + F_2 = 0 \\
&\kappa_3 = \frac{M_3}{EI} \\
&P_2 = \mu V_2 \\
&V_2' - \Omega_3 = 0 \\
&\Omega_3' = \dot{\kappa}_3
\end{aligned}
\tag{23}
$$

CHAPTER III

FULLY INTRINSIC EQUATIONS AND BOUNDARY CONDITIONS

Fully Intrinsic Equations are geometrically exact and constitute a closed set of equations, even though they include neither displacement nor rotation variables. They do not suffer from the singularities and infinite-degree nonlinearities normally associated with finite rotation variables. In fact, they have maximum degree of nonlinearity equal to two. In spite of these and other advantages of these equations, using them for problems with certain boundary conditions may not be straightforward. This chapter will examine the challenges of modeling various boundary conditions using fully intrinsic equations, thus helping future researchers to decide whether or not the fully intrinsic equations, are suitable for solving a specific problem and elucidating pathways for their application to more general problems. The material of this chapter is adapted from Refs. [57, 55].

In the fully intrinsic equations, the beam kinematics are described by velocity and angular velocity variables instead of displacement and rotation. In a rotating beam, even for a steady-state solution with no external forces or moments, the angular velocity is nonzero and the velocity varies along the beam. As it will be shown later, when using fully intrinsic equations to solve problems for rotating beams versus non-rotating beams, nonzero values for velocity and/or angular velocity can make a fundamental difference. This observation turns out to be quite helpful when solving fully intrinsic equations.

In this chapter, boundary conditions for steady-state solutions of non-rotating beams will be discussed, followed by a parallel discussion relating to rotating beams. Later, boundary conditions for the solution of the resulting eigenvalue problems will be discussed. Finally, a series of simple examples will be solved to illustrate different methods of applying boundary condition for fully intrinsic equations.

3.1 Boundary condition for steady-state solution of non-rotating beams

For static or steady-state problems, either natural boundary conditions in terms of force and moment (F and M) or geometric boundary conditions in terms of displacement (u) and direction cosine matrix (C^{Bi}) may be prescribed. When velocity and angular velocity (V and Ω) are not identically zero all along the beam, boundary conditions on displacement may replaced with equivalent boundary conditions on velocity, and those on rotation with equivalent conditions on angular velocity. When velocity and angular velocity (V and Ω) are identically zero all along the beam, geometric boundary conditions on displacement and rotation can be expressed in terms of integrals of strain (γ) and curvature (κ) measures using Eqs. (5) and (6) , thus keeping the formulation intrinsic.

3.1.1 Statically determinate structures

Clamped-free beam: The boundary conditions for a clamped-free beam are

$$\left.\begin{aligned} V_B &= 0 \\ \Omega_B &= 0 \end{aligned}\right\} \text{at the clamped end} \tag{24}$$

$$\left.\begin{aligned} F_B &= 0 \\ M_B &= 0 \end{aligned}\right\} \text{at the free end} \tag{25}$$

In this case, since every single equation has a boundary condition that can be associated with it, the problem will be always well posed [60]. Boundary conditions can prescribe zero or nonzero values at the end(s), e.g. consider a beam with a clamped root and a follower force at its tip.

Note that in a problem involving only static behavior, V and Ω are identically zero, and the structure is statically determinate. However, providing boundary conditions in terms of each may avoid singularities in the numerical procedure in case it contains velocity and angular velocity variables.

Clearly a clamped-free beam is the perfect problem to be solved with fully intrinsic equations.

Free-free beam: A practical problem of interest that is very well suited for the fully intrinsic equations is a flying wing [44, 11, 59], which can be modeled as a free-free beam. The boundary conditions for a flying wing are simply

$$\left.\begin{aligned} F_B &= 0 \\ M_B &= 0 \end{aligned}\right\} \text{at both free ends} \tag{26}$$

Although this looks very simple and intuitive, it actually is a very special case. The problem is physically well-posed only if the wing is under load (e.g. thrust, gravity and aerodynamic loads). In the presence of these kinds of forces, the velocity and angular velocity equations will have enough coupling with force and moment equations that the above boundary conditions on force and moment will allow the problem to be solved [44].

3.1.2 Statically indeterminate structures

Modeling statically indeterminate structures can be problematic with fully intrinsic equations, specially for non-rotating beams. When velocity and angular velocity are identically zero, Eqs. (2) will be trivial and will not provide any new information. Hence, the remaining equations, namely equations for equilibrium, Eqs. (1), and constitutive laws, Eqs. (3), are not sufficient to solve the problem. Certain strain-displacement equations will be needed in general. If the full nonlinear strain-displacement relations are used along with some measure of rotation, the advantages of the fully intrinsic equations are lost. To avoid this, the authors developed an alternative approach based on an incremental method [54]. This method is introduced, validated and applied in modeling joined-wing aircraft in Chapter 4

In many cases fully intrinsic equations in their original form can be used for statically indeterminate structures making use of Eqs. (5) and (6), especially when beam is initially curved or twisted. Here are some classical examples:

Pinned-pinned beam: A pinned-pinned beam with immovable ends is statically indeterminate, but if all equations that are trivially satisfied (i.e. zero equals zero) are excluded from the total set of governing equations, then the fully intrinsic equations in their original form can be used [10] (Otherwise one should provide appropriate boundary conditions for

trivially satisfied equations as well to avoid numerical difficulties). Note, however, that the boundary conditions depend on the type of pin at each end. The boundary conditions on force and moment are $F_i = 0$ or $M_i = 0$, where i is an appropriate axis (i =1, 2 or 3). The remaining boundary conditions are of the geometric type, and they can be applied in terms of relative displacement and rotation between the two ends of beam as follows:

$$\begin{aligned} \int_M^N r_i' dx_1 = r_i^N - r_i^M = \int_M^N C^{ib} e_1 dx_1 \\ \int_M^N (r_i + u_i)' dx_1 = r_i^N - r_i^M = \int_M^N C^{iB}(\gamma + e_1) dx_1 \end{aligned} \tag{27}$$

and

$$C_M^{iB} C_N^{Bi} = \Delta \tag{28}$$

where M and N identifies nodes at the two ends of the beam, and C_N^{iB} is the matrix of direction cosines of the inertial frame relative to the deformed beam cross-sectional frame at point N.

Clamped-clamped beam: For a clamped-clamped beam with immovable ends, all boundary conditions are geometric and are imposed using Eqs. (27) and (28). For instance, for a clamped-clamped beam with length L boundary conditions are

$$\int_0^L (r_i + u_i)' dx_1 = \int_0^L C^{iB}(\gamma + e_1) dx_1 = L \tag{29}$$

and

$$C_{x1=0}^{iB} C_{x1=L}^{Bi} = \Delta \tag{30}$$

In general, calculating an analytical Jacobian is very tedious for these equations, so in many cases the use of a numerical Jacobian is inevitable. Moreover, for beams with zero initial curvature and twist, finding a good initial guess for solving the resulting non-linear algebraic equations can be difficult. Hence, in many cases the incremental method may be advisable. This point will be illustrated in Chapter 4.

3.2 Beams restrained by translational and rotational springs

One straightforward method in modeling beam boundary conditions that are enforced by rotational and/or linear springs is to introduce displacement or rotation variables only at the

point(s) needed. This does not compromise any advantages of the fully intrinsic equations since the displacement and rotation are local, and they will only add a few extra variables. In most cases, the number of these extra variables is small compared to the total number of variables needed to model the beam. The same approach can be taken for modeling various joints. This approach was used in [8] to formulate equations for simulation of the ground vibration test for HALE aircraft. In case velocity and angular velocity variables are not identically zero, such as when modeling rotating blades or high-aspect-ratio wings undergo aerodynamic forces, it is possible to express such extra variables in terms of velocity and angular velocity variables, so that the equations and boundary conditions remain fully intrinsic. Examples 3.5.2 and 3.5.3 pertain to this.

3.3 Boundary conditions for steady-state solution of rotating beams

Rotating beams are ideal problems to be solved using fully intrinsic equations, since rotation implies nonzero values for V and Ω. In this case Eq. (2) is not trivially satisfied. Hence, for rotating beams, both statically determinate and indeterminate structures can be easily analyzed with fully intrinsic equations. A simple and quite fundamental example of a statically indeterminate structure may be found in a clamped-clamped rotating beam with immovable ends. Although it may not be of immense practical importance, it is a good example to illustrate how nonzero velocity and/or angular velocity helps in describing boundary conditions in the case of a statically indeterminate structure. This problem will be addressed as Example 3.5.1.

Problems involving a beam with at least one end subject only to natural boundary conditions, are actually easier to solve using the fully intrinsic equations since there will be at least one direct boundary condition in term of force or moment. Fully intrinsic equations are ideally suited for problems involving rotating beams with a free end, which have applications in modeling helicopter and wind turbine rotor blades.

3.4 Boundary conditions for linearized free-vibration analysis

A generalized eigenvalue problem can be derived by linearizing the discretized, fully intrinsic equations about a steady-state solution. Since the eigenvalue problem represents a dynamic

problem, fully intrinsic equations work well for all kinds of boundary conditions. One needs to enforce any displacement boundary conditions on velocity instead, and any rotation boundary conditions on angular velocity instead. With the use of velocity and angular velocity to describe geometric boundary conditions, however, rigid-body modes will not be eliminated from the results.

If the structure is supported by linear and/or rotational springs extra local variables can be introduced as was done in the steady-state case. In most cases, however, for dynamic problems these boundary conditions can be transformed so as to be written in terms of velocity and angular velocity variables instead. This allows the formulation to remain fully intrinsic. Examples 3.5.2 and 3.5.3 below follow this approach.

3.5 Examples

3.5.1 Ex. 1: Clamped-clamped rotating beam

Figure 4: Schematic of a clamped-clamped rotating beam

Consider a rotating, clamped-clamped beam, undergoing steady-state deformation without applied loads; Fig. 4 shows this structure. The only nonzero variables are axial force, the angular velocity component about an inertially fixed axis, and the velocity component perpendicular to the angular velocity vector. Assuming the beam has a prescribed angular velocity in the $\mathbf{B}_3 = \mathbf{b}_3 = \mathbf{i}_3$ direction given by ω_3, then it means that Ω_3, V_2 and F_1 are the only nonzero variables. The governing equations for this deceptively simple-looking problem are

$$\begin{aligned} \bar{\Omega}_3^+ &= 0 \\ \bar{F}_1^+ &= -\bar{\Omega}_3 \bar{V}_2 \\ \bar{V}_2^+ &= 1 + \bar{F}_1 \alpha^2 \end{aligned} \tag{31}$$

the boundary conditions of which are

$$\begin{aligned} \bar{V}_2(0) &= 0 \\ \bar{V}_2(1) &= 1 \\ \bar{\Omega}_3(0) &= 1 \end{aligned} \tag{32}$$

where

$$\begin{aligned} \bar{\Omega}_3 &= \frac{\Omega_3}{\omega_3} \\ \bar{F}_1 &= \frac{F_1}{\mu\omega_3^2 R^2} \\ \bar{V}_2 &= \frac{V_2}{R\omega_3} \\ x &= \frac{x_1}{R} \\ (\ )^+ &= \frac{d(\ )}{dx} \\ \alpha^2 &= \frac{\mu\omega_3^2 R^2}{EA} \end{aligned} \tag{33}$$

and where μ is the mass per unit length, and beam has length R. The axial strain γ_{11} is of the order of $\alpha^2 << 1$.

This set of equations actually has an analytical solution of the form

$$\begin{aligned} \bar{F}_1 &= \frac{\alpha \csc(\alpha)\cos(x\alpha) - 1}{\alpha^2} \\ \bar{V}_2 &= \csc(\alpha)\sin(x\alpha) \end{aligned} \tag{34}$$

Figs. 5 show axial force and velocity distribution for different values of α. Clearly, these quantities are insensitive to α when it is small.

3.5.2 Ex. 2: Pinned-free beam restrained by rotational spring

Figure 6 shows a pinned-free beam that is restrained by a rotational spring at the pinned end. The beam is assumed to be prismatic, of length R, rotating about an axis fixed in space parallel to $\mathbf{i}_3$ and subject to no external loads. Both steady-state and eigenvalue analyses are presented in terms of the fully intrinsic equations. Note that in the steady-state solution, because the rotational spring does not deform, the steady-state problem is governed by the same equations as for the clamped-free rotating beam example, and has identical boundary conditions and solution; see the section on the clamped-free beam.

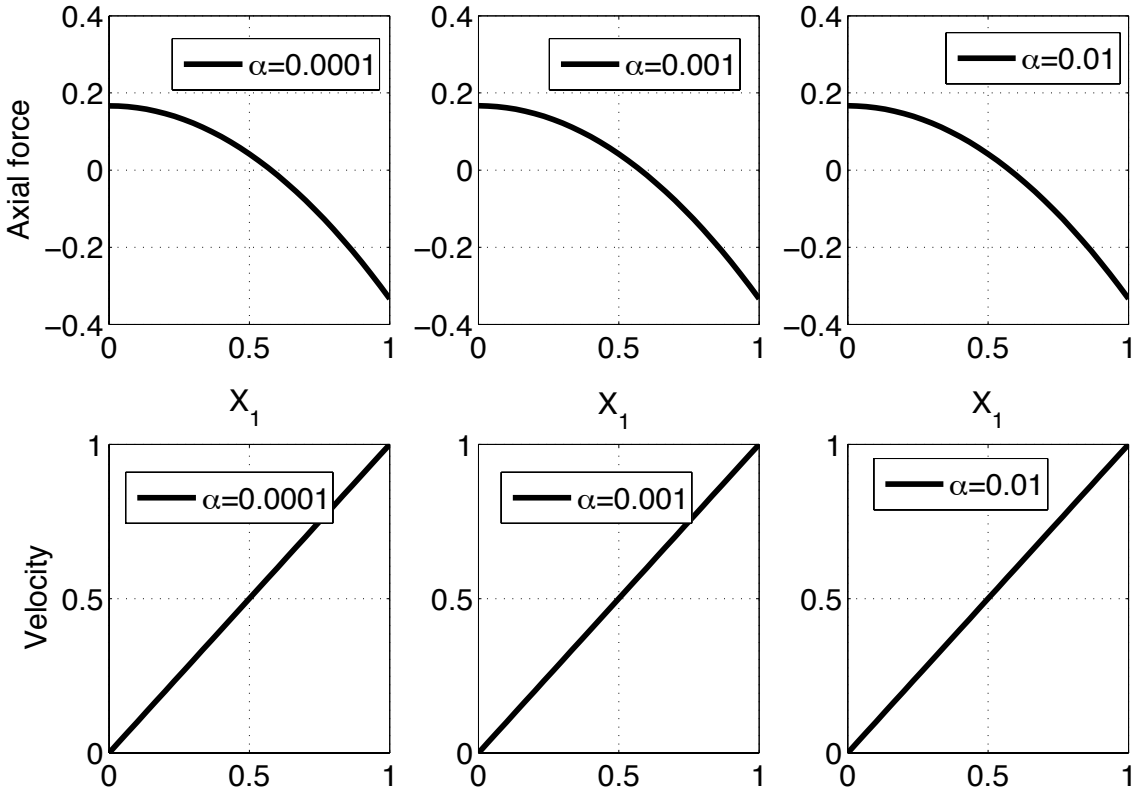

Figure 5: Dimensionless axial force and velocity distribution along a clamped-clamped rotating beam

Note that $\bar{\Omega}_3(x_1) = \omega_3$. Neglecting shear deformation, one obtains the linearized governing equations for the perturbation quantities $F_3(x_1,t)$, $M_1(x_1,t)$, $M_2(x_1,t)$, $V_3(x_1,t)$,

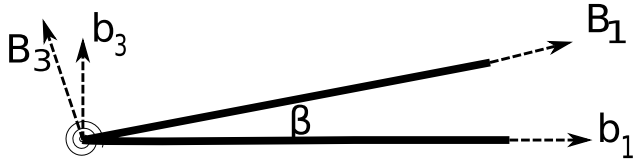

Figure 6: Schematic of a beam restrained by rotational spring

$\Omega_1(x_1,t)$ and $\Omega_2(x_1,t)$ as

$$\begin{aligned}
-\frac{M_2(x_1,t)\bar{F}_1(x_1)}{EI_2} - m\Omega_1(x_1,t)\bar{V}_2(x_1) - mV_3^{(0,1)}(x_1,t) + F_3^{(1,0)}(x_1,t) &= 0 \\
i_2\omega_3\Omega_2(x_1,t) - i_3\omega_3\Omega_2(x_1,t) - i_1\Omega_1^{(0,1)}(x_1,t) + M_1^{(1,0)}(x_1,t) &= 0 \\
-i_1\omega_3\Omega_1(x_1,t) + i_3\omega_3\Omega_1(x_1,t) - i_2\Omega_2^{(0,1)}(x_1,t) + M_2^{(1,0)}(x_1,t) - F_3(x_1,t)\left[1+\frac{\bar{F}_1(x_1)}{EA}\right] &= 0 \\
\Omega_2(x_1,t)\left[1+\frac{\bar{F}_1(x_1)}{EA}\right] + \frac{M_1(x_1,t)\bar{V}_2(x_1)}{GJ} + V_3^{(1,0)}(x_1,t) &= 0 \\
\frac{\omega_3 M_2(x_1,t)}{EI_2} - \frac{M_1^{(0,1)}(x_1,t)}{GJ} + \Omega_1^{(1,0)}(x_1,t) &= 0 \\
-\frac{\omega_3 M_1(x_1,t)}{GJ} - \frac{M_2^{(0,1)}(x_1,t)}{EI_2} + \Omega_2^{(1,0)}(x_1,t) &= 0
\end{aligned} \tag{35}$$

In Eqs. (35), $(\ )^{(0,1)}$ indicates a partial derivative with respect to time, $(\ )^{(1,0)}$ means a partial derivative with respect to x_1, and $\bar{(\ )}$ stands for steady-state values. Boundary conditions for this problem are

$$\begin{aligned}
F_3(R,t) &= 0 \\
M_1(R,t) &= 0 \\
M_2(R,t) &= 0 \\
V_3(0,t) &= 0 \\
M_2(0,t) &= k\beta \\
\dot{\Omega}_1(0,t) &= \omega_3\beta \\
\Omega_2(0,t) &= -\dot{\beta}
\end{aligned} \tag{36}$$

where β is the angle of rotation across the spring and is an extra variable in Eq. (36). Introducing an extra state variable such as β may be helpful when the value of β is of any particular interest in and of itself. Note, however, that β can be eliminated from the last

Table 1: Normalized natural frequencies of a pinned-free beam calculated with the fully intrinsic equations

Number of elements	η_1	η_2	η_3	η_4	η_5
10	10.0000	29.9285	69.9326	141.604	265.044
20	10.0000	29.5633	66.3656	124.914	208.664
40	10.0000	29.4737	65.5295	121.306	197.844
60	10.0000	29.4571	65.3770	120.659	195.951
80	10.0000	29.4514	65.3237	120.434	195.297
100	10.0000	29.4487	65.2991	120.330	194.995
Exact	10.0000	29.4439	65.2554	120.146	194.462

three equations of Eqs. (36), leading to a set of fully intrinsic boundary conditions

$$\begin{aligned} F_3(R,t) &= 0 \\ M_1(R,t) &= 0 \\ M_2(R,t) &= 0 \\ V_3(0,t) &= 0 \\ \dot{\Omega}_1(0,t) + \omega_3\Omega_2(0,t) &= 0 \\ \dot{M}_2(0,t) + k\Omega_2(0,t) &= 0 \end{aligned} \tag{37}$$

If the beam is not restrained with the spring, the last boundary condition reduces to $\dot{M}_2(0,t) = 0$, which implies that $M_2(0,t) = 0$ when rigid-body modes are excluded. Finally, letting $\omega_3 = 0$ will give the boundary conditions for a non-rotating beam. Table 1 shows the normalized natural frequencies η_i of a pinned-free beam calculated with the fully intrinsic equations. Results are compared with the exact solution [64]. These results are for $\lambda = 10$ where $\lambda = \omega_3\sqrt{mL^4/EI_2}$ and $\eta_i = v_i\sqrt{mL^4/EI_2}$.

3.5.3 Ex. 3: Beam restrained by longitudinal spring

Figure 7 shows a beam reinforced with a longitudinal spring attached to its root. The beam is under prescribed rotation as in the previous example ($\mathbf{\Omega} = \omega_3\mathbf{i}_3$). The complete set of

Figure 7: Schematic of a beam restrained by longitudinal spring attached to its root

fully intrinsic equations can be solved along with boundary conditions

$$\begin{aligned}
\bar{\Omega}_{1,2}(0,t) &= 0 \\
\bar{\Omega}_3(0,t) &= 1 \\
\bar{V}_1(0,t) &= \frac{d(\bar{u})}{d\tau} \\
\bar{V}_{2,3}(0,t) &= 0 \\
\bar{F}_i(1,t) &= 0 \text{ for } i\text{=1,2,3} \\
\bar{M}_i(1,t) &= 0 \text{ for } i\text{=1,2,3} \\
\bar{F}_1(0,t) &= \lambda\bar{u}
\end{aligned} \tag{38}$$

where $\tau = \omega_3 t$ is dimensionless time, R is the length of the beam, u is the spring stretch (assuming an unstretched length of zero), $\bar{u} = u/R$, λ is $k/(\mu\omega_3^2 R)$, k is the spring stiffness, μ is the beam mass per unit length and the normalization of other variables for Eq. (38) is the same as used above for Eq. (33).

For dynamic solution Eq. (38) can be written in fully intrinsic form by eliminating $\bar{u}$, so that

$$\begin{aligned}
\bar{\Omega}_{1,2}(0,t) &= 0 \\
\bar{\Omega}_3(0,t) &= 1 \\
\bar{V}_{2,3}(0,t) &= 0 \\
\bar{F}_{1,2,3}(1,t) &= 0 \\
\bar{M}_{1,2,3}(1,t) &= 0 \\
\frac{d(\bar{F}_1(0,t))}{d\tau} &= \lambda\frac{d(\bar{V}_1(0,t))}{d\tau}
\end{aligned} \tag{39}$$

This configuration can be unstable when the angular speed is sufficiently high [27]. The real and imaginary parts of the eigenvalues are shown in Fig. 8, revealing a static

(buckling) type instability for a beam with the properties given in Table 2. Figure 9 shows the steady-state axial force distribution for this problem at $\omega_3 = 20$ rad/s.

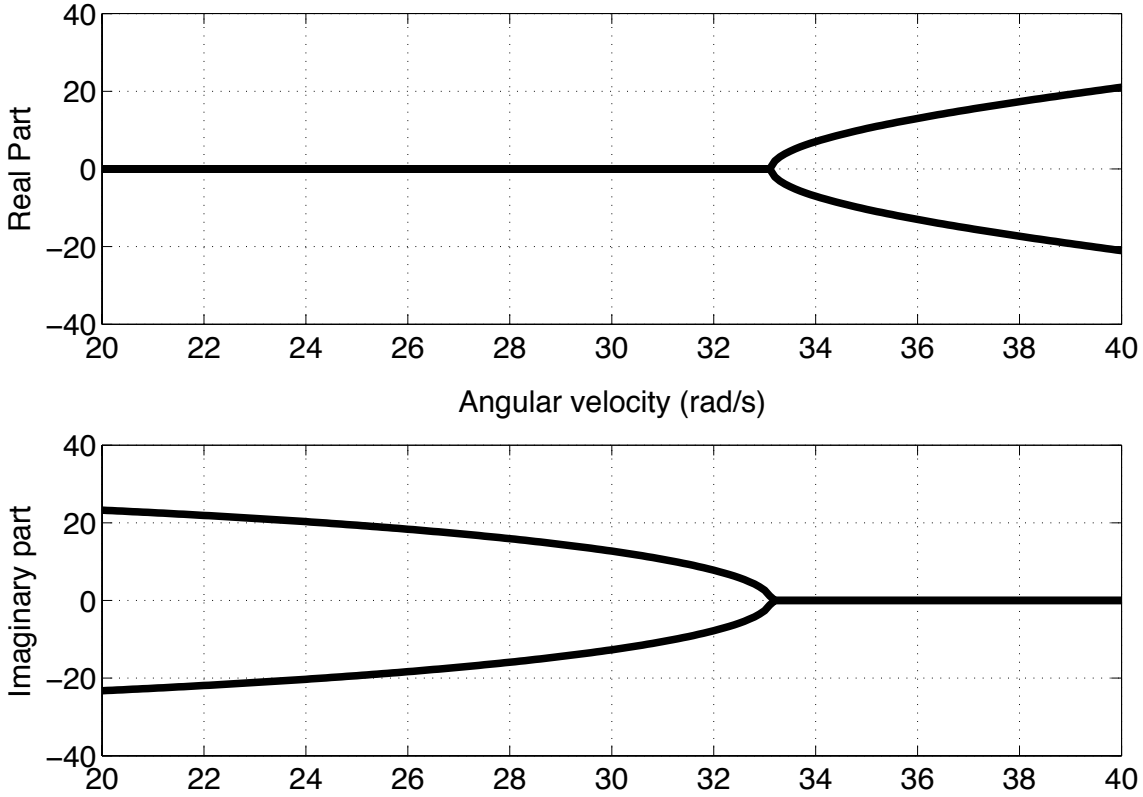

Figure 8: Real and imaginary parts of the eigenvalues versus angular speed for a rotating beam restrained at its root by a longitudinal spring.

In the next chapter, the application of the fully intrinsic equations on statically indeterminate structures will be studied. In this regard, an incremental method will be developed and validated. Finally, the incremental method will be applied to a joined-wing aircraft configuration.

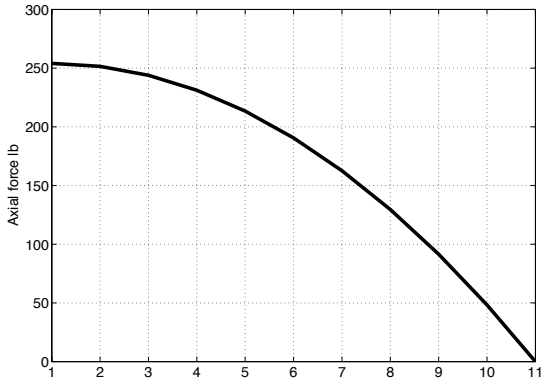

Figure 9: Steady-state axial force distribution for example 3.5.3

Table 2: Beam properties, English units

Length	10 [ft]
Axial stiffness	0.1322×10^7 [lb]
Torsional stiffness	0.0221×10^5[lb ft^2]
Out-of-plane bending stiffness	0.0172×10^5 [lb ft^2]
In-plane bending stiffness	1.0989×10^5 [lb ft^2]
Mass per unit length	0.0127 [slug/ft]
Mass polar moment of inertia per unit length	0.0011 [ft^3]
Spring stiffness	100 [lb/ft]

CHAPTER IV

INCREMENTAL METHOD FOR STRUCTURAL ANALYSIS OF JOINED-WING AIRCRAFT

This chapter is mostly adopted from Refs. [42]. Joined-wing aircraft are characterized by statically indeterminate structures: structures with multiple load paths. A new way of analyzing these configurations is introduced in this chapter. This new formulation is based on the fully intrinsic equations, which introduce neither singularities nor infinite-degree nonlinearities caused by finite rotation. The formulation makes use of an incremental form of the kinematical equations, which preserves the main advantages of the fully intrinsic equations. The method is applied and verified for a joined-wing structure.

The special case of joined-wing aircraft presents a challenge for a fully intrinsic formulation because of its static indeterminacy. The absence of displacement and rotation variables can create a mismatch in the number of quantities that must be specified at the boundaries versus the information known there. For example, a formulation with velocity variables instead of displacement variables presents no challenge in a dynamic formulation, but in a static problem where all velocities are zero, there is insufficient information at the boundaries to solve the resulting equations. Hence, analysis of a joined-wing aircraft using the fully intrinsic equations boils down to analyzing static behavior of a statically indeterminate structure. In this chapter the solution of statically indeterminate structures using the fully intrinsic equations is addressed, and the method is applied to joined-wing aircraft as an example of its capability. Here a slightly different definition of intrinsic equations is used, which means a formulation without displacement and rotation parameterization.

4.1 Theory

4.1.1 Boundary condition challenges

Figure 10 shows sketch of four different configurations of HALE aircraft structures. These configurations can be easily modeled as a combination of beams. Configurations (1) and

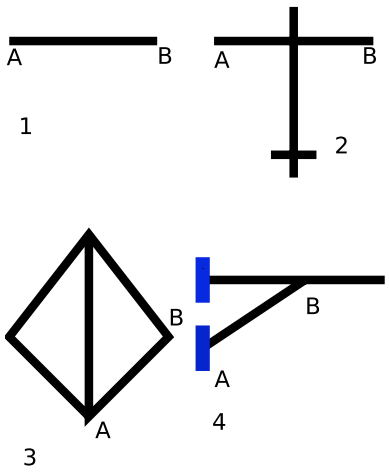

Figure 10: Sketch of different configurations of HALE aircraft structures

(2) show a flying wing and a conventional aircraft, respectively. These configurations are statically determinate so that in the static case, the equilibrium equation (i.e. Eqs. 1 and 2) are sufficient to solve these structures. Moreover, in a flying wing or a conventional configuration, there are sufficient boundary conditions on force, moment, velocity and angular velocity because each beam has at least one free end. This facilitates numerical solutions for solving steady-state problems [55]. On the other hand, configurations (3) and (4) are joined-wing configurations and obviously statically indeterminate structures. In static analysis when velocity and angular velocity are identically zero, Eqs. (3) and (4) are trivially satisfied. Since these structures are statically indeterminate, equilibrium equations are insufficient for solving for the behavior. An incremental method is introduced to overcome this difficulty associated with finding the static equilibrium state of statically indeterminate structures such as joined-wing aircraft. After the equilibrium state is found, the fully intrinsic equations can be linearized about the static equilibrium state for dynamical analysis. The incremental method is based on repeatedly solving linear systems of equations as the load is gradually increased. The governing equations for dynamics of small motions about the equilibrium state can then be reduced to a generalized eigenvalue problem.

4.1.2 Incremental method

The incremental method consists of sets of linear equations of motion, which are obtained by dropping all time derivatives from the governing equations and linearizing them. Thus,

the fully intrinsic equations of motion become

$$\begin{aligned}
\check{F}'_B + \widetilde{\check{K}}_B \check{F}_B - \widetilde{\check{F}}_B \check{K}_B + \check{f}_B &= \widetilde{\check{\Omega}}_B \check{P}_B - \widetilde{\check{P}}_B \check{\Omega}_B \\
\check{M}'_B + \widetilde{\check{K}}_B \check{M}_B - \widetilde{\check{M}}_B \check{K}_B + (\widetilde{e_1} + \widetilde{\check{\gamma}}) \check{F}_B - \widetilde{\check{F}}_B \check{\gamma} + \check{m}_B &= \widetilde{\check{\Omega}}_B \check{H}_B - \widetilde{\check{H}}_B \check{\Omega}_B + \widetilde{\check{V}}_B \check{P}_B - \widetilde{\check{P}}_B \check{V}_B
\end{aligned} \tag{40}$$

and the fully intrinsic kinematical equations are

$$\begin{aligned}
\check{V}'_B + \widetilde{\check{K}}_B \check{V}_B - \widetilde{\check{V}}_B \check{K}_B + (\widetilde{e_1} + \widetilde{\check{\gamma}}) \check{\Omega}_B - \widetilde{\check{\Omega}}_B \check{\gamma} &= 0 \\
\check{\Omega}'_B + \widetilde{\check{K}}_B \check{\Omega}_B - \widetilde{\check{\Omega}}_B \check{K}_B &= 0
\end{aligned} \tag{41}$$

making use of the linear constitutive equations

$$\begin{Bmatrix} \check{\gamma} \\ \check{\kappa} \end{Bmatrix} = \begin{bmatrix} R & S \\ S^T & T \end{bmatrix} \begin{Bmatrix} \check{F}_B \\ \check{M}_B \end{Bmatrix} \tag{42}$$

and generalized velocity-momentum equations

$$\begin{Bmatrix} \check{P}_B \\ \check{H}_B \end{Bmatrix} = \begin{bmatrix} \mu\Delta & -\mu\tilde{\xi} \\ \mu\tilde{\xi} & I \end{bmatrix} \begin{Bmatrix} \check{V}_B \\ \check{\Omega}_B \end{Bmatrix} \tag{43}$$

In these equations the $\bar{(\ )}$ quantities are known from the previous loading step, and the $\check{(\ )}$ quantities are the unknowns at each step. An exception to this is that $\check{f}$ and $\check{m}$ are small, specified increments of applied force and moment.

In the incremental method, equations that govern incremental displacement and rotation must also be included. These have the form

$$\begin{aligned}
\check{\gamma} &= \check{q}'_B + \widetilde{\check{K}}_B \check{q}_B + (\widetilde{e_1} + \widetilde{\check{\gamma}}) \check{\psi}_B \\
\check{\kappa} &= \check{\psi}'_B + \widetilde{\check{K}}_B \check{\psi}_B
\end{aligned} \tag{44}$$

Although incremental displacements and rotations are introduced, the governing equations are linear, and there are neither infinite-degree nonlinearities nor singularities associated with introducing finite rotation. Hence, the two main advantages of the fully intrinsic equations, namely avoiding nonlinearities of orders higher than second and avoiding singularities, are kept.

Equations 40 – 44 should be solved at each step due to an incremental loading. After each step all variables except the direction cosine matrix, $\bar{q}$ and $\bar{\psi}$ are updated using relations

of the form

$$\bar{X}_{new} = \bar{X}_{old} + \check{X} \tag{45}$$

while q and ψ do not need to be updated. The direction cosine matrix, C, is updated using

$$C_{new} = \left(\Delta - \tilde{\check{\psi}}\right) C_{old} \tag{46}$$

It turns out that this first-order update for direction cosine matrix, C, has been sufficient in all cases run so far; however, a second-order update may be used if desired. Displacement can be calculated by either using Eq. 6b at the end of the solution procedure as a post-processing task or by updating a variable such as $\bar{q}$ with $\check{q}$ at every step, so that

$$\bar{q}_{new} = \bar{q}_{old} + C^{iB}\check{q} \tag{47}$$

4.1.2.1 Modeling gravity using the incremental method

As mentioned before, externally applied loads should be applied incrementally in this method. These externally applied loads $\check{f}$ and $\check{m}$ may include any kind of applied forces, such as gravity, thrust, or aerodynamic forces. For modeling dead forces such as gravity, the direction cosine matrix plays an essential role. A distributed gravitational force is written as

$$f_{g_i} = -\mu g \mathbf{i}_3 \cdot \mathbf{B}_i \quad \text{so that} \quad f_g = -\mu g C^{Bi} e_3 \tag{48}$$

Thus, the incremental term may be written as

$$\check{f}_g = -(\check{\mu g}) C^{Bi} e_3 - \mu g \check{C}^{Bi} e_3 \tag{49}$$

Here $(\check{\mu g}) C^{Bi} e_3$ is an inhomogeneous term, with $(\check{\mu g})$ as the incremental value in each step; and $\mu g \check{C}^{Bi} e_3$ is a homogeneous term. Note that $C^{Bi} = C^{Bb} C^{bi} = C C^{bi}$ and $\check{C} = -\tilde{\check{\psi}} C$. If there is an offset between the center of mass and the beam reference line, then the moment caused by gravity can be developed in the same way, viz.,

$$m_{g_i} = [\xi_\alpha \mathbf{B}_\alpha \times (-\mu g \mathbf{i}_3)] \cdot \mathbf{B}_i \quad \text{so that} \quad m_g = -\mu g \tilde{\xi} C^{Bi} e_3 \tag{50}$$

where α takes on values 2 and 3, and repeated indices are summed over their range. Thus, the incremental term may be written as

$$\check{m}_g = -(\check{\mu g}) \tilde{\xi} C^{Bi} e_3 - \mu g \tilde{\xi} \check{C}^{Bi} e_3 \tag{51}$$

4.1.2.2 Modeling aerodynamic force/moment in the incremental method

A two-dimensional (2D) aerodynamic model is used to calculate the aerodynamic loads generated by wings and control surfaces such as flaperons. The quasi-steady aerodynamic model has been changed to an unsteady model by adding the effect of induced flow from the 2D induced flow model of Peters et al. [48], along with apparent mass/inertia terms in the force and moment equations. The final force and moment equations, respectively, take the form [44]

$$f_a = \rho b \begin{Bmatrix} 0 \\ -(C_{l_0} + C_{l_\beta}\beta)V_T V_{a_3} + C_{l_\alpha}(V_{a_3} + \lambda_0) - C_{d_0} V_T V_{a_2} \\ (C_{l_0} + C_{l_\beta}\beta)V_T V_{a_2} - 2\pi \dot{V}_{a_3} b/2 - C_{l_\alpha} V_{a_2}(V_{a_3} + \lambda_0) + 2\pi V_{a_2}\Omega_{a_1} b/2 - C_{d_0} V_T V_{a_3} \end{Bmatrix} \tag{52}$$

and

$$m_a = 2\rho b^2 \begin{Bmatrix} (C_{m_0} + C_{m_\beta}\beta)V_T^2 - C_{m_\alpha} V_T V_{a_3} - b\frac{C_{l_\alpha}}{8} V_{a_2}\Omega_{a_1} - 2\pi(\frac{b^2}{32}\dot{\Omega}_{a_1} - \frac{b}{8}\dot{V}_{a_3}) \\ 0 \\ 0 \end{Bmatrix} \tag{53}$$

and where V_{a_2} and V_{a_3} are the second and third elements of velocity vector in the aerodynamic frame of reference, and $V_T = \sqrt{V_{a_2}^2 + V_{a_3}^2}$.

For the steady-state solution, the applied aerodynamic force and moment will be, respectively,

$$f_a = \rho b \begin{Bmatrix} 0 \\ -(C_{l_0} + C_{l_\beta}\beta)V_T V_{a_3} + C_{l_\alpha} V_{a_3}^2 - C_{d_0} V_T V_{a_2} \\ (C_{l_0} + C_{l_\beta}\beta)V_T V_{a_2} - C_{l_\alpha} V_{a_2} V_{a_3} + 2\pi V_{a_2}\Omega_{a_1} b/2 - C_{d_0} V_T V_{a_3} \end{Bmatrix} \tag{54}$$

and

$$m_a = 2\rho b^2 \begin{Bmatrix} (C_{m_0} + C_{m_\beta}\beta)V_T^2 - C_{m_\alpha} V_T V_{a_3} - \frac{b}{8} C_{l_\alpha} V_{a_2}\Omega_{a_1} \\ 0 \\ 0 \end{Bmatrix} \tag{55}$$

So for the incremental method $\check{f}_a$ and $\check{m}_a$ are

$$\check{f}_{a_1} = 0 \tag{56}$$

$$
\begin{aligned}
\check{f}_{a_2} = & -b\rho\left[\frac{C_{d_0}\bar{V}_{a_2}^2}{\bar{V}_T}+\frac{\left(C_{l_0}+\beta C_{l_\beta}\right)\bar{V}_{a_3}\bar{V}_{a_2}}{\bar{V}_T}+C_{d_0}\bar{V}_T\right]\check{V}_{a_2}+ \\
& -b\rho\left[\frac{\left(C_{l_0}+\beta C_{l_\beta}\right)\bar{V}_{a_3}^2}{\bar{V}_T}-2C_{l_\alpha}\bar{V}_{a_3}+\frac{C_{d_0}\bar{V}_{a_2}\bar{V}_{a_3}}{\bar{V}_T}+\left(C_{l_0}+\beta C_{l_\beta}\right)\bar{V}_T\right]\check{V}_{a_3} \\
\check{f}_{a_3} = & \; b\rho\left[\frac{\left(C_{l_0}+\beta C_{l_\beta}\right)\bar{V}_{a_2}^2}{\bar{V}_T}-\frac{C_{d_0}\bar{V}_{a_3}\bar{V}_{a_2}}{\bar{V}_T}+\left(C_{l_0}+\beta C_{l_\beta}\right)\bar{V}_T-C_{l_\alpha}\bar{V}_{a_3}+\pi b\bar{\Omega}_{a_1}\right]\check{V}_{a_2}+ \\
& b\rho\left[-\frac{C_{d_0}\bar{V}_{a_3}^2}{\bar{V}_T}+\frac{\left(C_{l_0}+\beta C_{l_\beta}\right)\bar{V}_{a_2}\bar{V}_{a_3}}{\bar{V}_T}-C_{d_0}\bar{V}_T-C_{l_\alpha}\bar{V}_{a_2}\right]\check{V}_{a_3}+ \\
& b^2\rho\pi\bar{V}_{a_2}\check{\Omega}_{a_1} \\
\check{m}_{a_1} = & \; 2b^2\rho\left[2\left(C_{m_0}+\beta C_{m_\beta}\right)\bar{V}_{a_2}-\frac{1}{8}bC_{l_\alpha}\bar{\Omega}_{a_1}\right]\check{V}_{a_2}+ \\
& 2b^2\rho\left[2\left(C_{m_0}+\beta C_{m_\beta}\right)\bar{V}_{a_3}-C_{m_\alpha}\bar{V}_T\right]\check{V}_{a_3}- \\
& \frac{1}{4}b^3\rho C_{l_\alpha}\bar{V}_{a_2}\check{\Omega}_{a_1} \\
\check{m}_{a_2} = & \; 0 \\
\check{m}_{a_3} = & \; 0
\end{aligned}
\tag{57, 58, 59}
$$

where $\bar{V}_T = \sqrt{\bar{V}_{a_2}^2 + \bar{V}_{a_3}^2}$. Applied loads f_a and m_a should be transferred to the B frame by use of

$$
\begin{aligned}
f_B = & C_a f_a \\
m_B = & C_a m_a + C_a \tilde{y}_{ac} f_a
\end{aligned}
\tag{60}
$$

4.1.3 Stability Analysis

A generalized eigenvalue problem can be derived by linearizing the discretized, fully intrinsic equations about a constant steady-state solution, which is computed using the incremental method. Since the eigenvalue problem represents a dynamics problem, the fully intrinsic equations work well for the vibration and forced response of statically indeterminate structures. One needs simply to replace displacement boundary conditions with boundary conditions on velocity, and similarly replace boundary conditions on rotation with boundary conditions on angular velocity. With the use of velocity and angular velocity to describe geometric boundary conditions, however, zero frequencies may occur which are due to lack of enough boundary conditions on force and moment in a statically indeterminate structure.

4.2 Verification of Incremental Method

In this section the incremental method is first verified by study of a clamped-clamped non-rotating beam under a distributed load and a clamped-clamped rotating beam. As a second example, the incremental method is verified against available experimental results [17] and against results obtained from the mixed formulation [43], including eigenvalues. The simple aerodynamic model is verified against that found in NATASHA (Nonlinear Aeroelastic Trim And Stability for HALE Aircraft). Validation studies of NATASHA may be found in Ref. [60]. Here the incremental method is applied to a clamped-free beam, and results obtained are compared against those of NATASHA.

All units are in an English system in which mass is in slugs, time in seconds, force in pounds and length in feet, unless otherwise specified. However, the input data and results obtained and reported in the paper are correct in any *consistent* system of units.

4.2.1 Verification of the incremental method for a clamped-clamped non-rotating beam

In this example we illustrate the benefit of the incremental method in obtaining a steady-state solution for a statically indeterminate structure. For this purpose the easiest example is a clamped-clamped beam. This problem is inherently nonlinear and serves our purpose very well. A beam with the properties given in Table 3 is undergoing a distributed transverse force of 10 lb/ft as shown in Fig. 11.

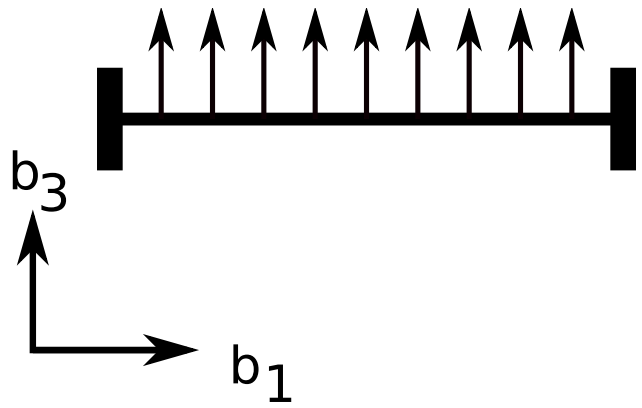

Figure 11: A clamped-clamped beam under distributed load

This problem has been solved by a mixed formulation, in which the geometric boundary

Table 3: Beam properties, English units

Length	20 [ft]
Axial stiffness	1.322×10^6 [lb]
Torsional stiffness	0.0221×10^5 [lb ft^2]
Out-of-plane bending stiffness	0.0172×10^5 [lb ft^2]
In-plane bending stiffness	1.0989×10^5 [lb ft^2]
Mass per unit length	0.0127 [slug/ft]
Mass polar moment of inertia per unit length	0.0011 [ft^3]

conditions are expressed easily in terms of displacement and rotation parameters. Table 4 shows values of axial force (F_1), bending moment (M_2) and transverse displacement (u_3) at mid-span and shear force (F_3) at the beam root for different number of elements using a mixed formulation. This problem is also solved by the present incremental method. Results from the incremental method are compared with those of the mixed formulation with 400 elements. The out-of-plane bending moment and axial force have their maximum values at mid-span, and the shear force has its maximum value at the clamped ends. Hence the errors are calculated for axial force and bending moment at mid-span and shear force at the root ($x_1 = 0$).

Figures 12, 13 and 14 show convergence of the axial and shear forces and bending moment using the incremental method. As one can see clearly, the error decreases rapidly with an increase in the number of steps. Figures 15 and 16 show axial and out-of-plane displacement for the problem at hand. Displacements are calculated by virtue of Eq. 47. Also, Figs. 17, 18 and 19 show axial force, shear force and out-of-plane bending moment for the problem at hand.

Orthogonality of the direction matrix is of concern in this method, since the right hand side of Eq. (46) is not an orthogonal matrix. However, the error is small at each step. One needs to check the norm of $C^{Bi}C^{iB} - \Delta$ at given steps (not necessarily at each step). In the case of large error, one should enforce the orthogonality constraint on C, (possibly by use of Lagrangian multiplier).[1] The norm of $C^{Bi}C^{iB} - \Delta$, which should be identically zero,

[1]Technical discussion with Prof. Oliver Bauchau and Prof. Mayuresh Patil is gratefully acknowledged.

Table 4: Mixed formulation results for clamped-clamped beam, English units

Number of elements	F_1 [lb]	M_2 [lb ft]	F_3 [lb]	u_3 [ft]	CPU time [s]
10	1040.2602	16.5395	99.8917	0.3572	1.5223
20	1046.0439	16.3877	99.9122	0.3556	3.0232
30	1047.1065	16.3518	99.9168	0.3553	4.3092
40	1047.4775	16.3387	99.9185	0.3552	5.7290
50	1047.6490	16.3325	99.9194	0.3552	7.6265
80	1047.8347	16.3257	99.9202	0.3551	16.9257
100	1047.8775	16.3242	99.9204	0.3551	22.4882
120	1047.9008	16.3233	99.9205	0.3551	28.9707
140	1047.9148	16.3228	99.9206	0.3551	40.9120
160	1047.9239	16.3225	99.9207	0.3551	52.5070
400	1047.9489	16.3215	99.9208	0.3551	506.3128

was checked for each node at the end of solution procedure. It approximates zero with a very good accuracy, so that orthogonality of direction cosine matrix is preserved in the incremental method. Better accuracy is always achievable by using a second-order update of C at each step instead of a first-order update. Table 5 shows the two-norm of $C^{Bi}C^{iB} - \Delta$ for the problem under consideration with 20 elements and for different numbers of steps when a first-order update is used for updating the direction cosine matrix. Table 6 shows the same quantity for a second-order update. The small errors for the first-order update do not seem to have any deleterious effect on the overall accuracy of the results, and the errors in the second-order update approach machine precision. Figure 20 shows computational time vs. number of steps for different number of elements. Figure 21 shows the relative error of the first three natural frequencies of a clamped-clamped beam, calculated using the fully intrinsic equations, versus the number of elements. Clearly, convergence is taking place as the number of elements grows.

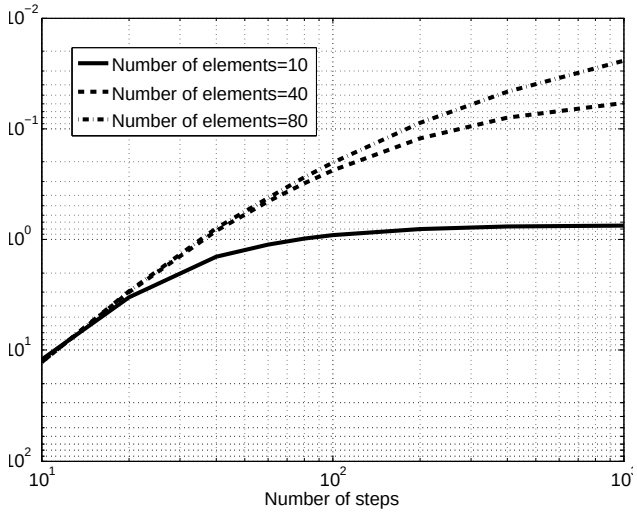

Figure 12: Convergence of axial force

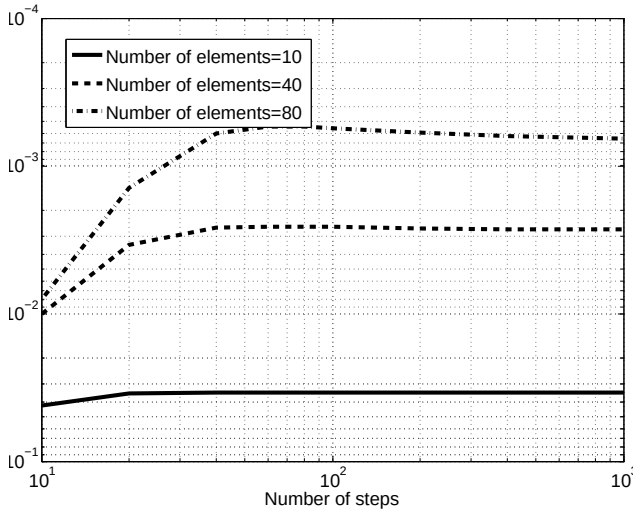

Figure 13: Convergence of shear force

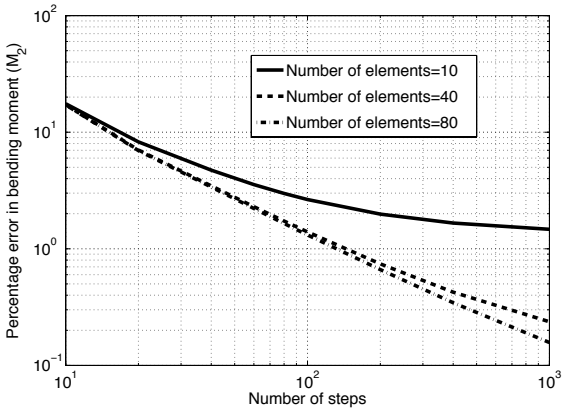

Figure 14: Convergence of out of plane bending moment

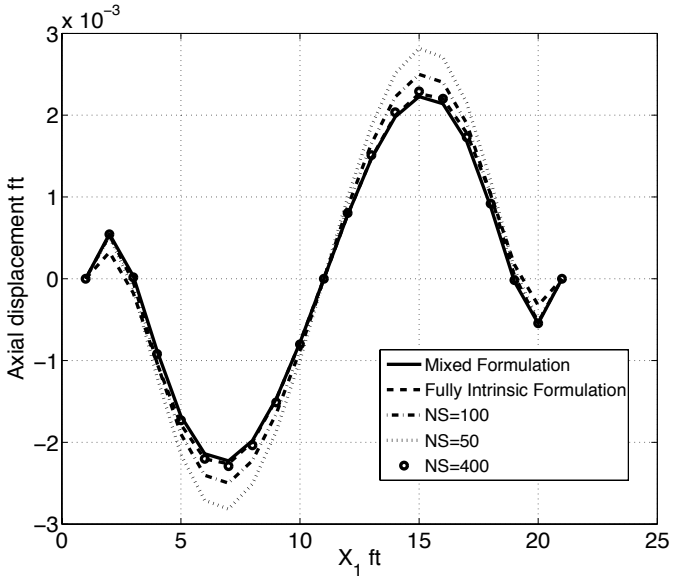

Figure 15: Axial displacement along the beam

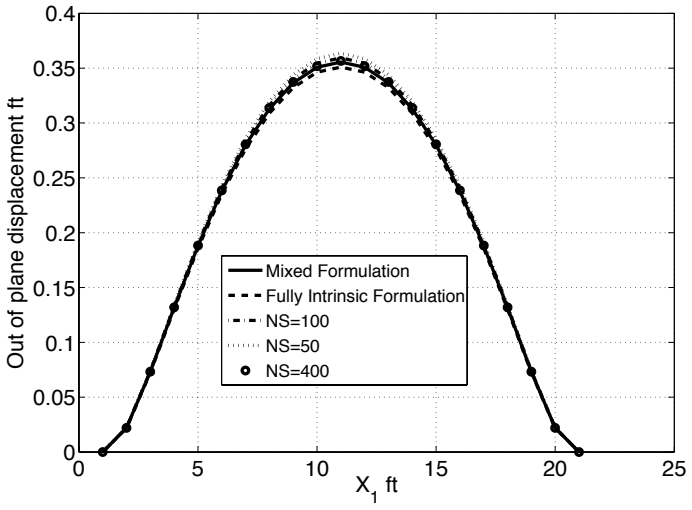

Figure 16: Out of plane displacement along the beam

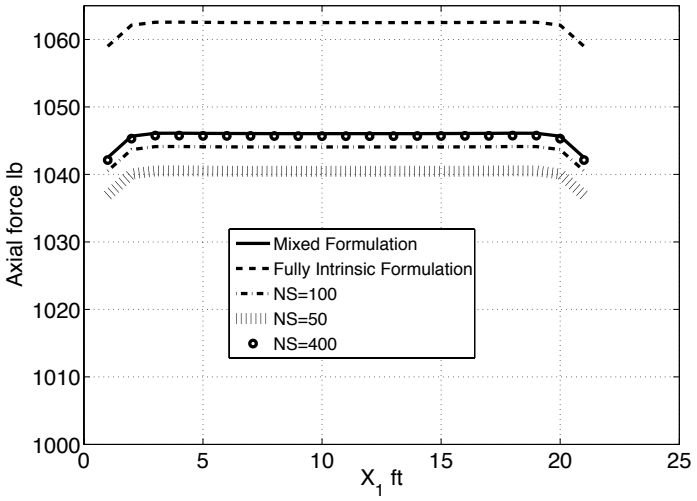

Figure 17: Axial force along the beam

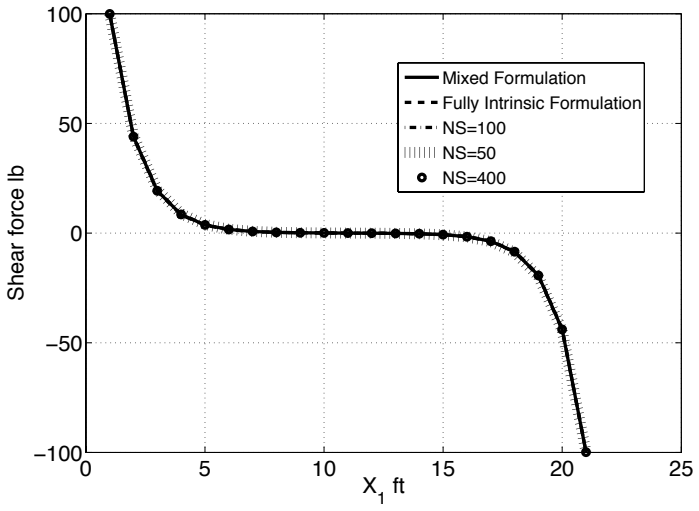

Figure 18: Shear force along the beam

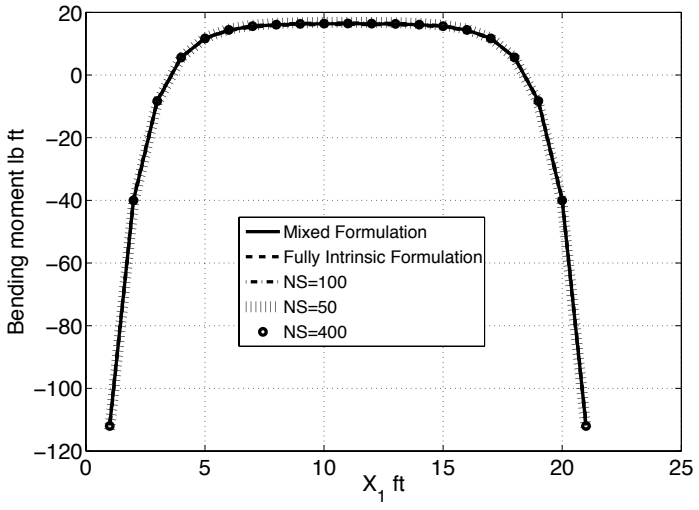

Figure 19: Out of plane bending moment along the beam

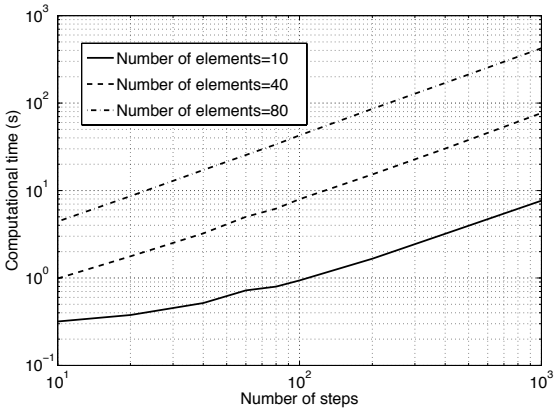

Figure 20: Computational time for incremental method

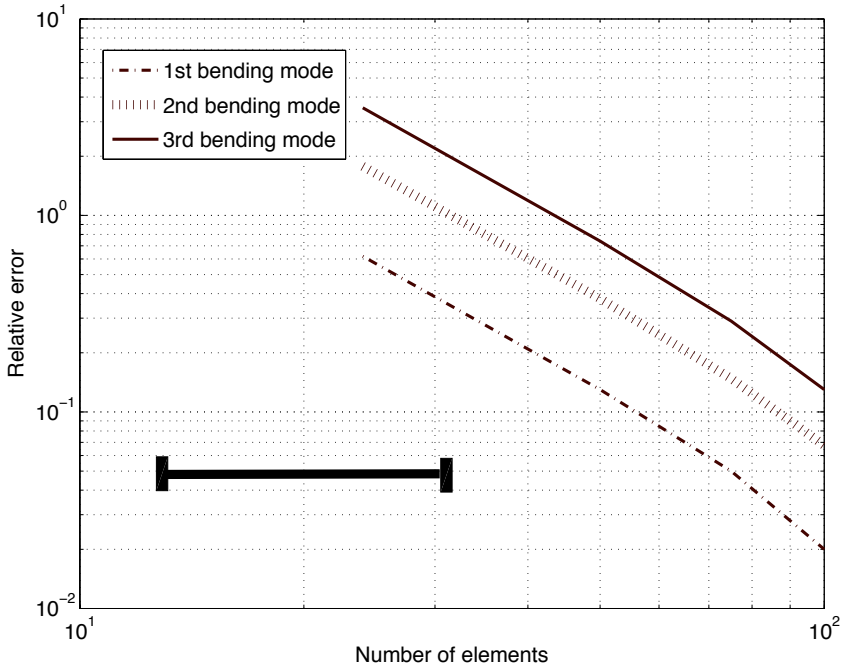

Figure 21: Relative error in natural frequency of a clamped-clamped beam versus number of elements

Table 5: Orthogonality error for C^{Bi} using first-order update

Node number	10 steps	100 steps	1000 steps
Node 1	0	0	0
Node 2	6.66E-007	6.65E-008	6.65E-009
Node 3	1.89E-006	1.89E-007	1.89E-008
Node 4	2.90E-006	2.90E-007	2.90E-008
Node 5	3.35E-006	3.35E-007	3.35E-008
Node 6	3.20E-006	3.19E-007	3.19E-008
Node 7	2.57E-006	2.56E-007	2.56E-008
Node 8	1.69E-006	1.69E-007	1.69E-008
Node 9	8.37E-007	8.36E-008	8.36E-009
Node 10	2.23E-007	2.22E-008	2.22E-009
Node 11	0	0	0
Node 12	2.23E-007	2.22E-008	2.22E-009
Node 13	8.37E-007	8.36E-008	8.36E-009
Node 14	1.69E-006	1.69E-007	1.69E-008
Node 15	2.57E-006	2.56E-007	2.56E-008
Node 16	3.20E-006	3.19E-007	3.19E-008
Node 17	3.35E-006	3.35E-007	3.35E-008
Node 18	2.90E-006	2.90E-007	2.90E-008
Node 19	1.89E-006	1.89E-007	1.89E-008
Node 20	6.66E-007	6.65E-008	6.65E-009
Node 21	0	0	0

Table 6: Orthogonality error for C^{Bi} using second-order update

Node number	10 steps	100 steps	1000 steps
Node 1	0	0	0
Node 2	1.11E-014	8.88E-016	5.77E-015
Node 3	8.93E-014	1.11E-015	1.24E-014
Node 4	2.10E-013	1.67E-015	2.55E-015
Node 5	2.81E-013	4.44E-016	1.03E-014
Node 6	2.56E-013	1.33E-015	7.22E-015
Node 7	1.65E-013	2.22E-016	1.61E-014
Node 8	7.17E-014	1.67E-015	2.31E-014
Node 9	1.73E-014	4.44E-016	1.51E-014
Node 10	8.88E-016	7.77E-016	6.33E-015
Node 11	0	0	0
Node 12	8.88E-016	7.77E-016	6.33E-015
Node 13	1.73E-014	4.44E-016	1.51E-014
Node 14	7.17E-014	1.67E-015	2.31E-014
Node 15	1.65E-013	2.22E-016	1.61E-014
Node 16	2.56E-013	1.33E-015	7.22E-015
Node 17	2.81E-013	4.44E-016	1.03E-014
Node 18	2.10E-013	1.67E-015	2.55E-015
Node 19	8.93E-014	1.11E-015	1.24E-014
Node 20	1.11E-014	8.88E-016	5.77E-015
Node 21	0	0	0

4.2.2 Verification of the incremental method for a clamped-clamped rotating beam

A clamped-clamped rotating beam (Fig. 22) can be solved with fully intrinsic equation, although this structure is statically indeterminate. Actually there is an analytical solution [55] for a rotating, clamped-clamped beam with no external loading. Assuming the beam has a prescribed angular velocity in the $\mathbf{B}_3 = \mathbf{b}_3 = \mathbf{i}_3$ direction given by ω_3, then it means that Ω_3, V_2 and F_1 are the only non-zero variables. Here this problem is solved with incremental method and results of incremental method is compared versus analytical results. Governing equations can be found in Refs. [55, 57]. The analytical solution for this problem is as follows:

$$\begin{aligned} \bar{F}_1 &= \frac{\alpha \csc(\alpha) \cos(x\alpha) - 1}{\alpha^2} \\ \bar{V}_2 &= \csc(\alpha) \sin(x\alpha) \end{aligned} \tag{61}$$

where

$$\begin{aligned} \bar{\Omega}_3 &= \frac{\Omega_3}{\omega_3} \\ \bar{F}_1 &= \frac{F_1}{\mu \omega_3^2 R^2} \\ \bar{V}_2 &= \frac{V_2}{R\omega_3} \\ x &= \frac{x_1}{R} \\ (\,)^+ &= \frac{d(\,)}{dx} \\ \alpha^2 &= \frac{\mu \omega_3^2 R^2}{EA} \end{aligned} \tag{62}$$

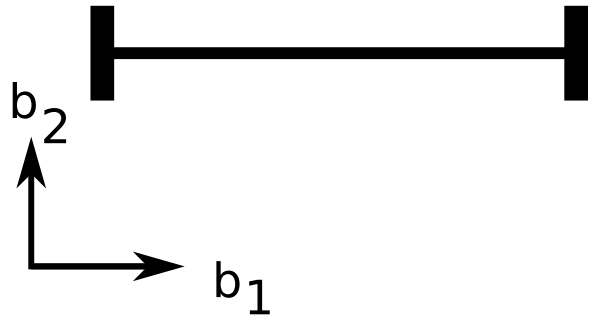

Figure 22: Top view of a clamped-clamped rotating beam; angular velocity is about $\mathbf{b}_3$.

Figure 23 shows convergence of axial force to analytical solution for different number of elements versus number of steps. Figure 24 shows computational time for different number

of elements and number of steps. Figure 25 and 26 shows axial force and velocity (in chordwise direction) for 500 steps and 40 elements. Analytical solution and incremental method solution are right on top of each other. For these results $\alpha^2 = 0.00346$.

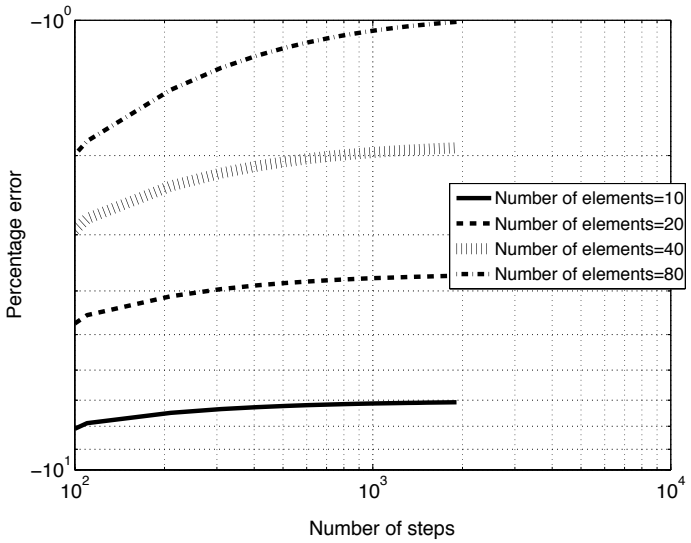

Figure 23: Axial force convergence for a clamped-clamped rotating beam

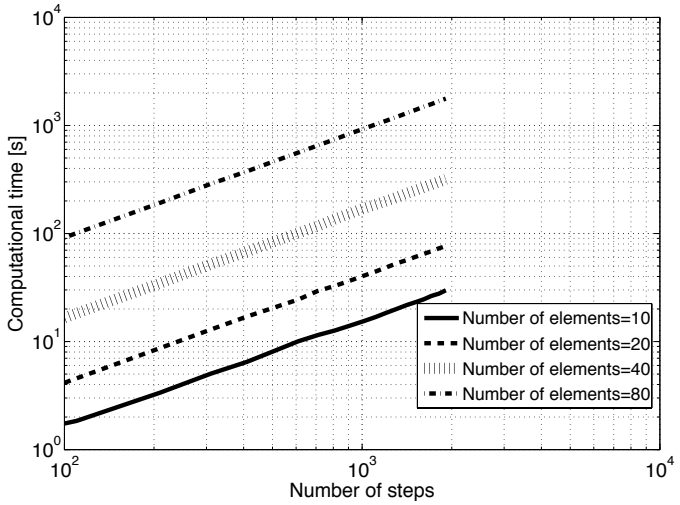

Figure 24: Computational time for a clamped-clamped rotating beam

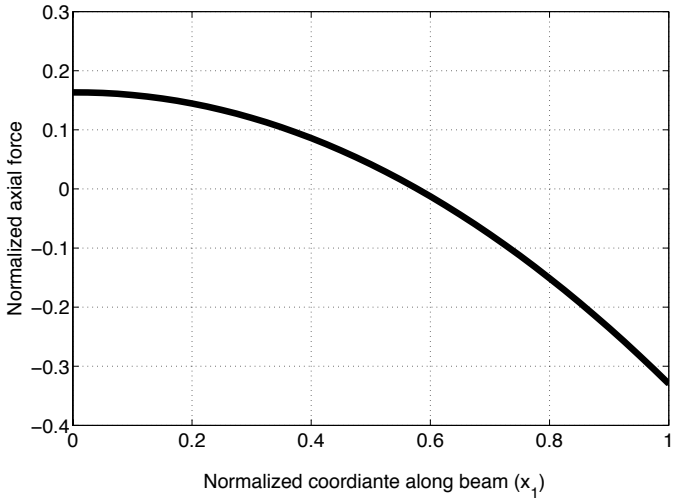

Figure 25: Axial force distribution for clamped-clamped rotating beam

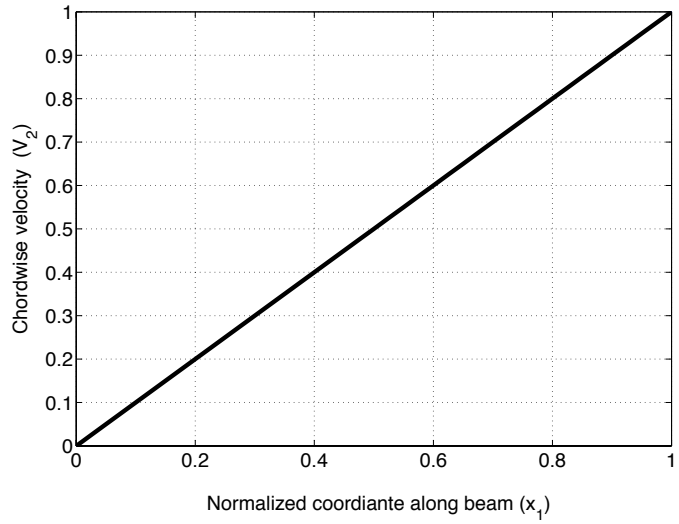

Figure 26: Chordwise velocity distribution for a clamped-clamped rotating beam

4.2.3 Validation vs. experimental results

Figure 27 is the case considered throughout this section. Table 7 shows the structural properties of this configuration. Figure 30 shows the joint deflection versus a varying tip load. Results from the incremental method are in excellent agreement with those of the mixed formulation [43]. Neither formulation perfectly matches the experimental data [17] after a certain point because of yielding of the joint [43]. Figure 31 shows the tip deflection of the same structure under varying tip load for the incremental method, the mixed formulation and experimental results. The mixed formulation and the incremental method are again in excellent agreement with each other and are both close to the experimental results. Figure 32 shows the out-of-plane bending deflection of the main wing of the same structure under a constant load distribution [43]. Again results from the mixed formulation and the incremental method are in excellent agreement.

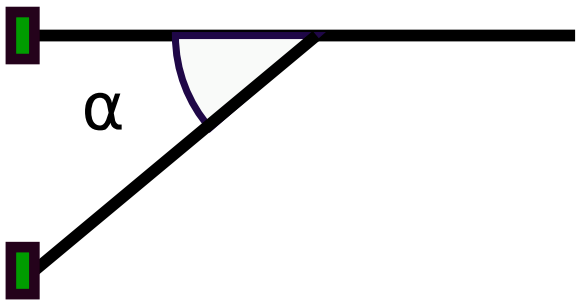

Figure 27: Joined wing configuration under study

Table 7: Beam properties for configuration in Fig. 27, English units

Length of front wing	20 [in]
Length of aft wing	10 [in]
Joint position	10 [in]
α	60°
Torsional stiffness	2214 [lb in^2]
Out-of-plane bending stiffness	1.1017×10^5 [lb in^2]
In-plane bending stiffness	1721.4 [lb in^2]
Mass per unit length	0.012675 [slug/in]
Mass moment of inertia per unit length for out-of-plane bending	1.6504×10^{-5} [in^3]
Mass moment of inertia per unit length for in-plane bending	0.0010728 [in^3]
Polar mass moment of inertia per unit length	0.0010728 [in^3]

4.2.4 Verification of the incremental method for a non-planar joined-wing configuration

The incremental method is also verified for a nonplanar joined-wing configuration versus results obtained from the mixed formulation [43]. Figure 28 shows transverse tip and joint deflection of a joined wing versus magnitude of tip load, respectively. This test case is exactly the same as one in Ref. [43]. 100 steps are used to achieve these results.

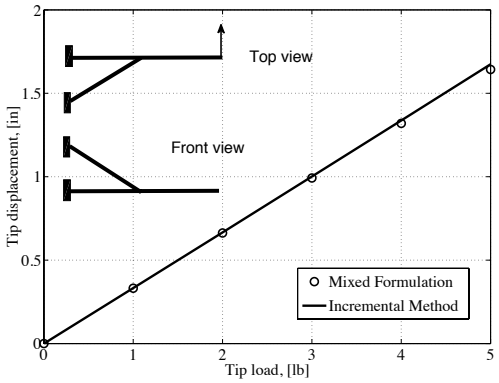

Figure 28: Tip deflection for nonplanar joined-wing configuration

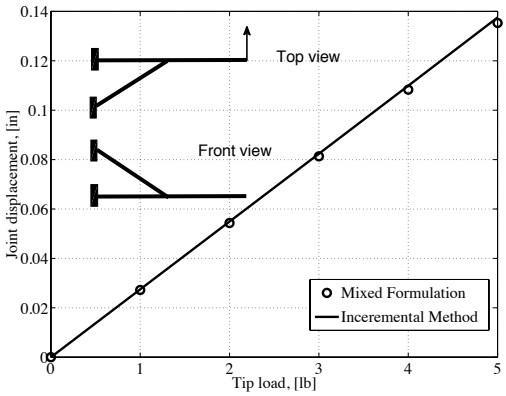

Figure 29: Joint deflection for nonplanar joined-wing configuration

4.2.5 Verification of Eigenvalue Analysis vs. Mixed formulation

For validation of the eigenvalue solver, a structure the same as in Figure 27 with properties the same as in Table 7 is used. The structure is under a constant distributed follower force of 0.5 lb./ft. 100 steps were used to solve the steady-state equations. 80 elements were used

in the front wing and 40 in the aft. Table 8 shows the first five eigenvalues calculated with the incremental method based on fully intrinsic equations and with the mixed formulation.

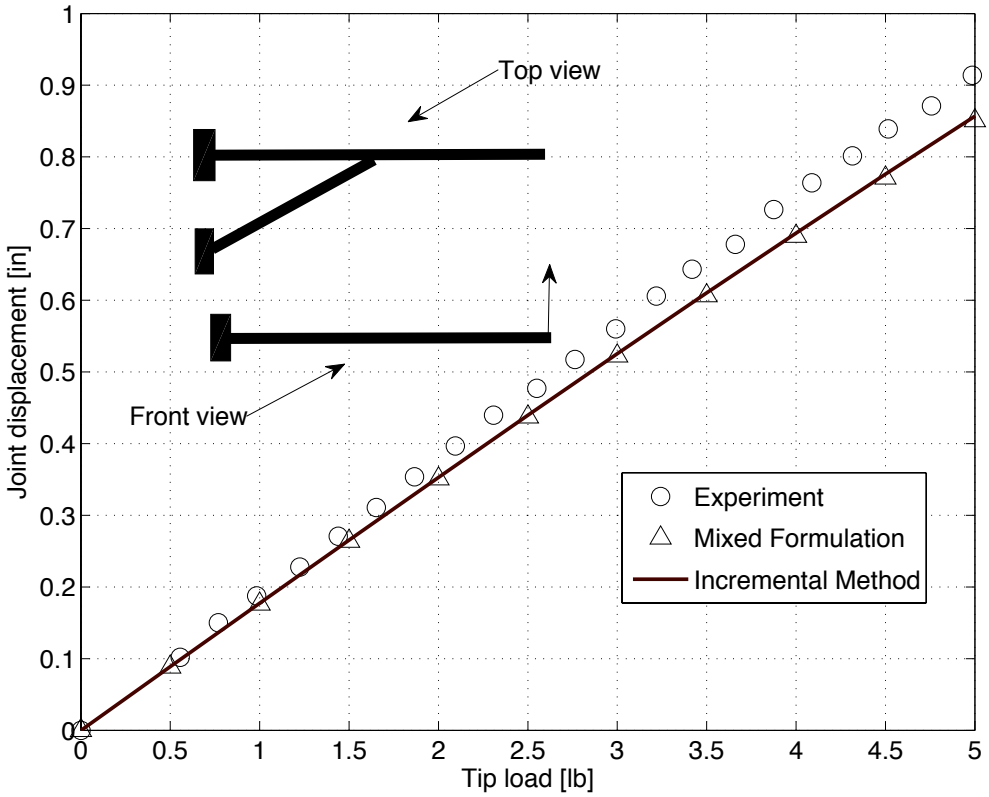

Figure 30: Joint deflection

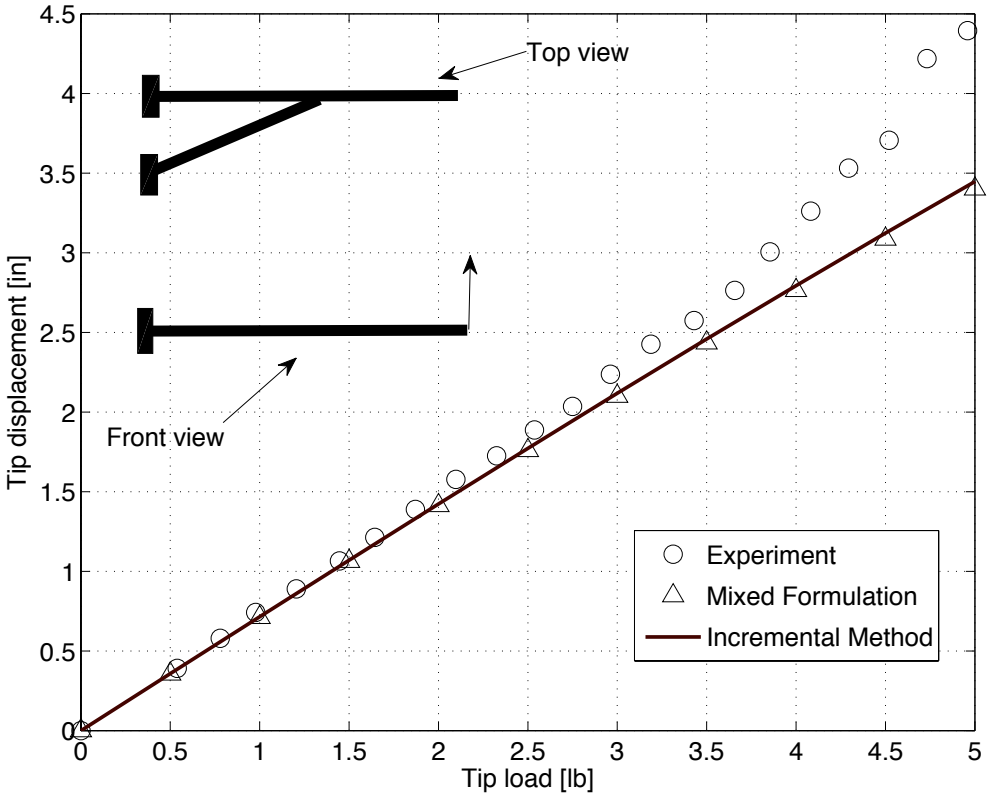

Figure 31: Tip deflection

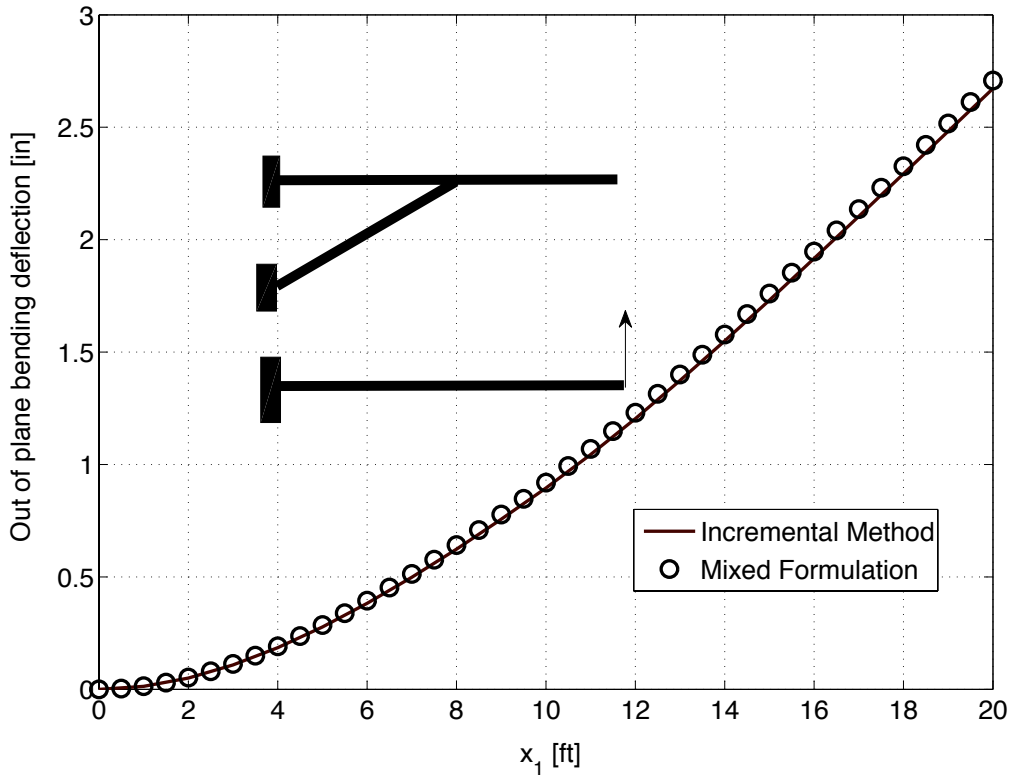

Figure 32: Out-of-plane bending deflection

Table 8: Eigenvalues [rad/s] from fully intrinsic equations vs. those from mixed formulation

Fully intrinsic equations	Mixed formulation	Percentage difference
5.03	5.02	-0.27
19.97	19.91	-0.28
57.58	57.38	-0.35
58.32	58.27	-0.10
94.07	93.34	-0.77

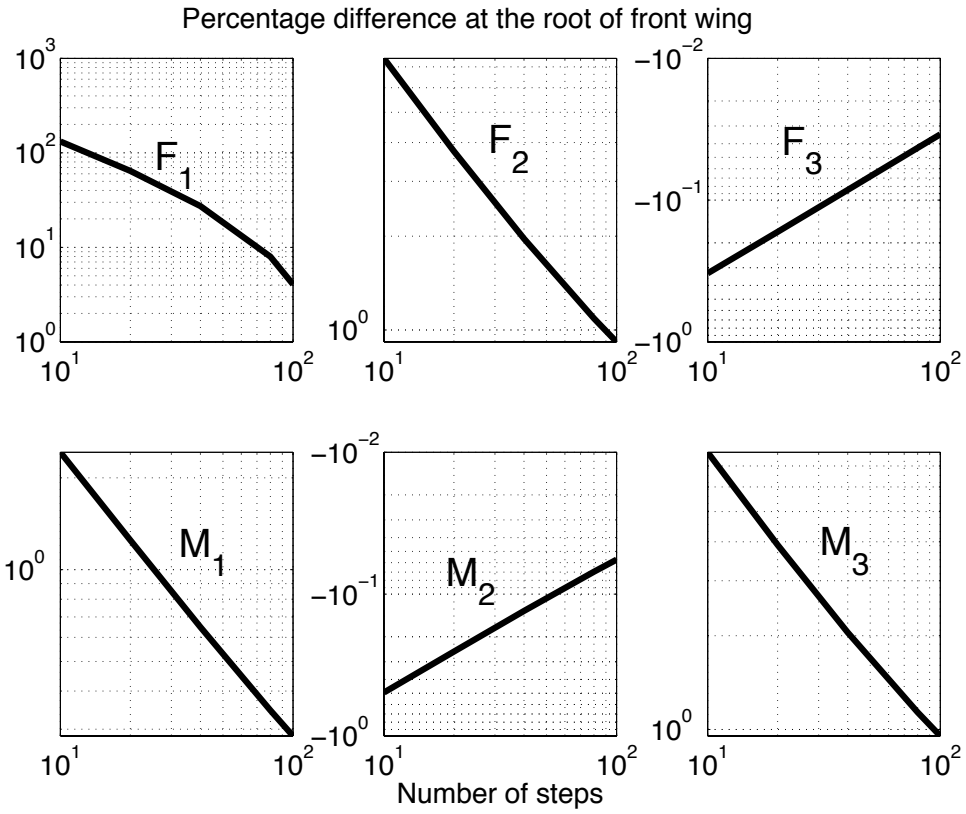

Figure 33: Convergence of force and moments values to the mixed formulation solution vs. number of steps for front wing root

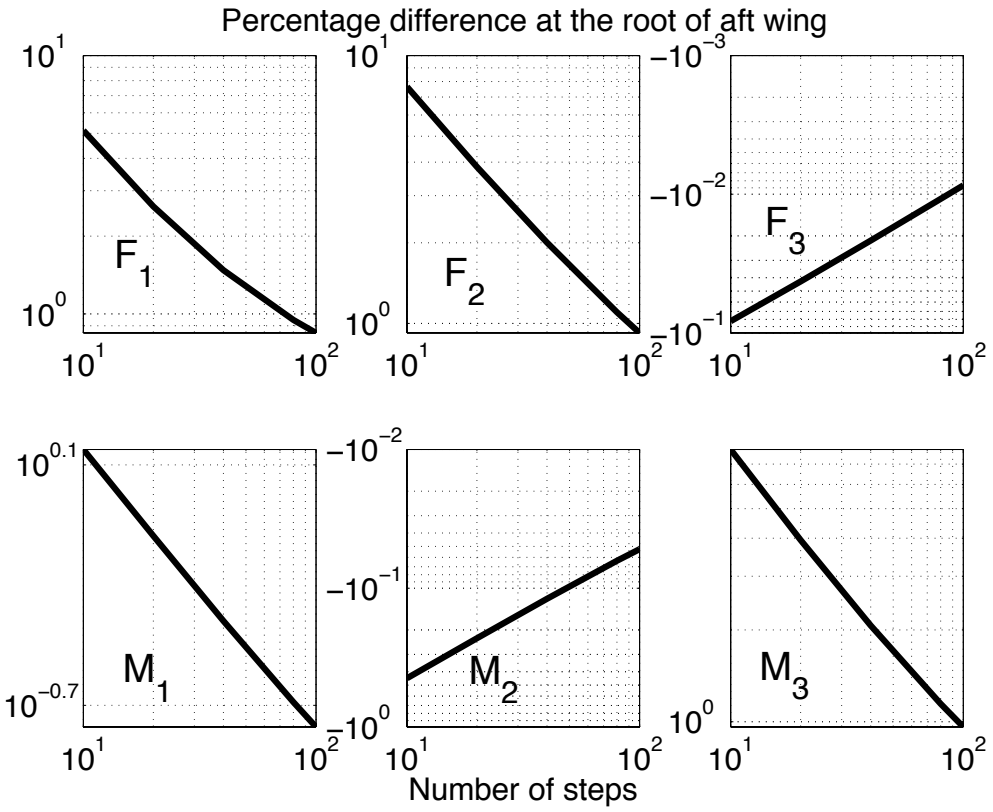

Figure 34: Convergence of force and moment values to the mixed formulation solution vs. number of steps for aft wing root

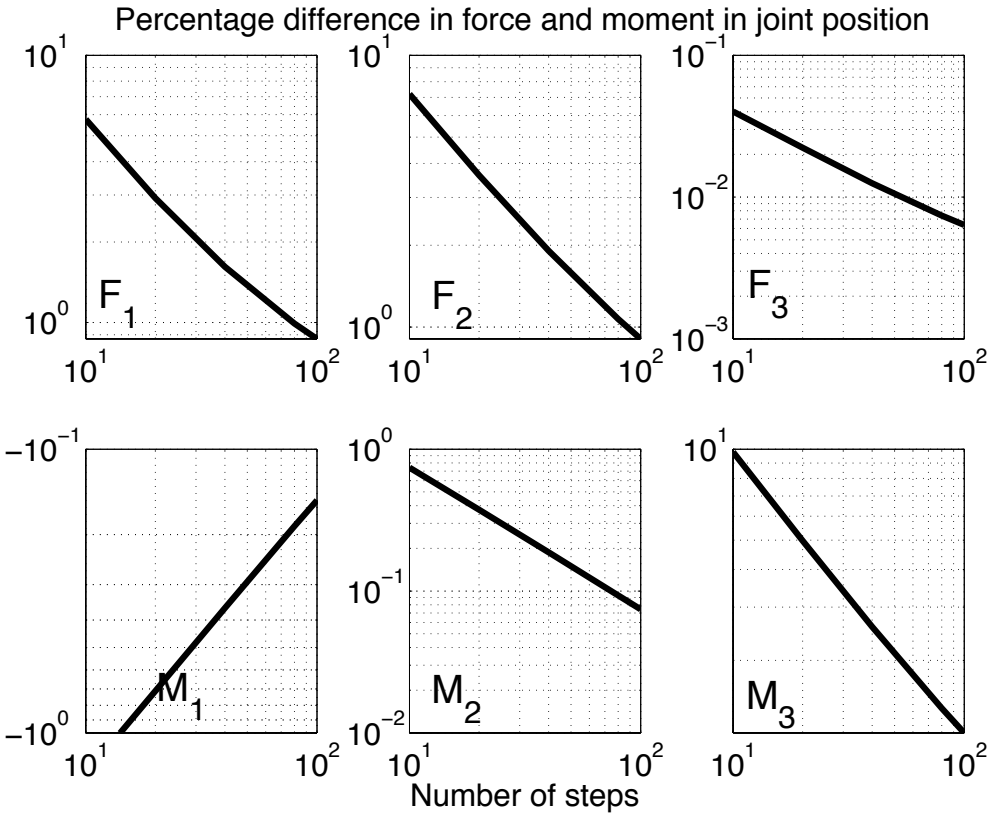

Figure 35: Convergence of force and moment values to the mixed formulation solution vs. number of steps for joint

4.2.6 Convergence study

Because the incremental method works by solving a sequence of linear problems to find the steady-state solution for a joined-wing structure under a specific loading, the number of steps plays a specific role. The clamped-clamped example shows a very good convergence rate. Here convergence of incremental method for the same structure as Fig. 27 is studied. Table 7 shows structural properties for the problem at hand. Both wings are loaded with a follower force in the $\mathbf{B}_3$ direction, having a constant magnitude of 0.5 lb. Results are compared with those using the mixed formulation for the same number of finite elements. The front and aft wing roots and the joint (i.e. the junction) are critical points in this configuration. Figures 33, 34 and 35 show percentage difference with respect to mixed formulation's results for these three points as number of steps increases.

There are three critical points in this configuration, i.e. the two clamped ends and the joint position; see Fig. 27. Figures 33, 34 and 35 show the convergence of force and moment measure numbers in the $\mathbf{B}_i$ basis at these three critical points. For this study the front wing has 40 elements and the aft wing 20. The mixed formulation results for the same number of finite elements is taken as the reference solution. Determination of the axial force (F_1) is an inherently nonlinear process for a joined-wing configuration, and it thus takes more steps to converge to the exact solution. Figures 36 and 37 show the distributions of internal force and moment in front and aft wing for the same problem. The number of steps for these results is 100.

4.2.7 Verification of aerodynamics model implementation vs. NATASHA

Implementation of the aerodynamic formulation in the incremental method is verified by a comparison of the results for a clamped-free beam under an aerodynamic load with results from NATASHA. Table 9 shows aerodynamic properties of the beam. Figure 38 shows the force and moment distributions for this beam. The good agreement attests to the correctness of the aerodynamic modeling in the incremental method.

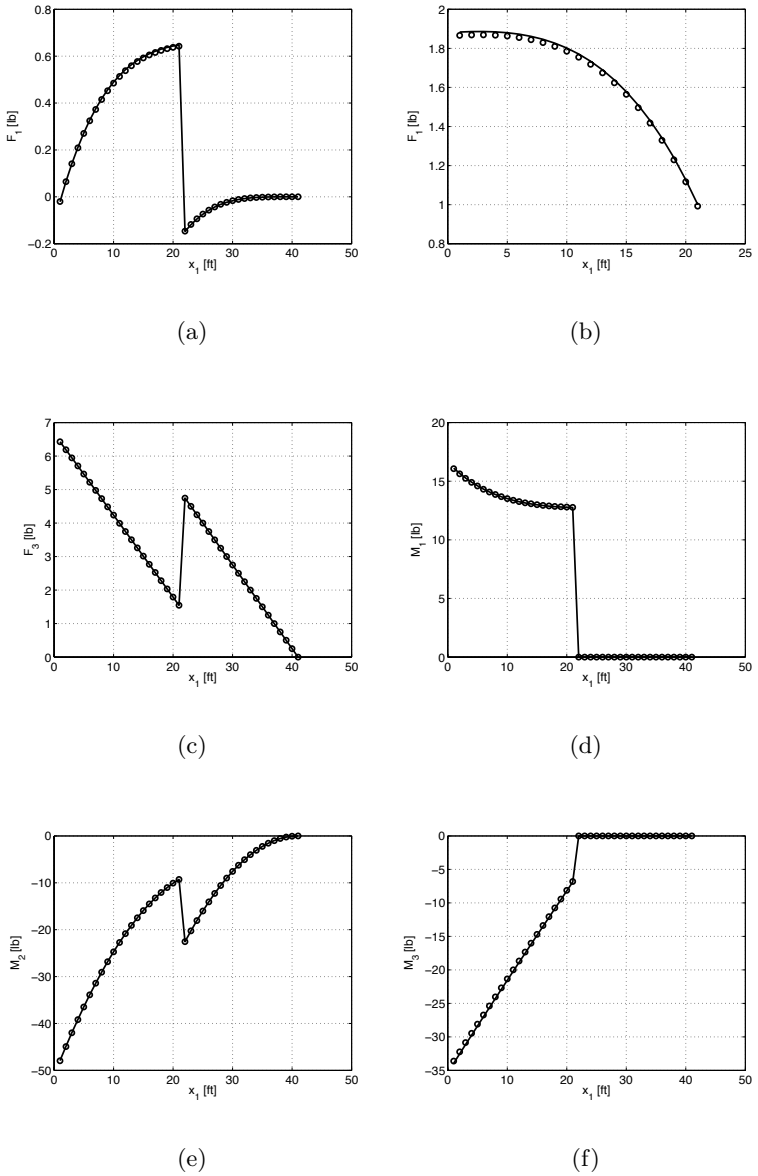

Figure 36: Force (a – c) and moment (d – f) distributions in front wing

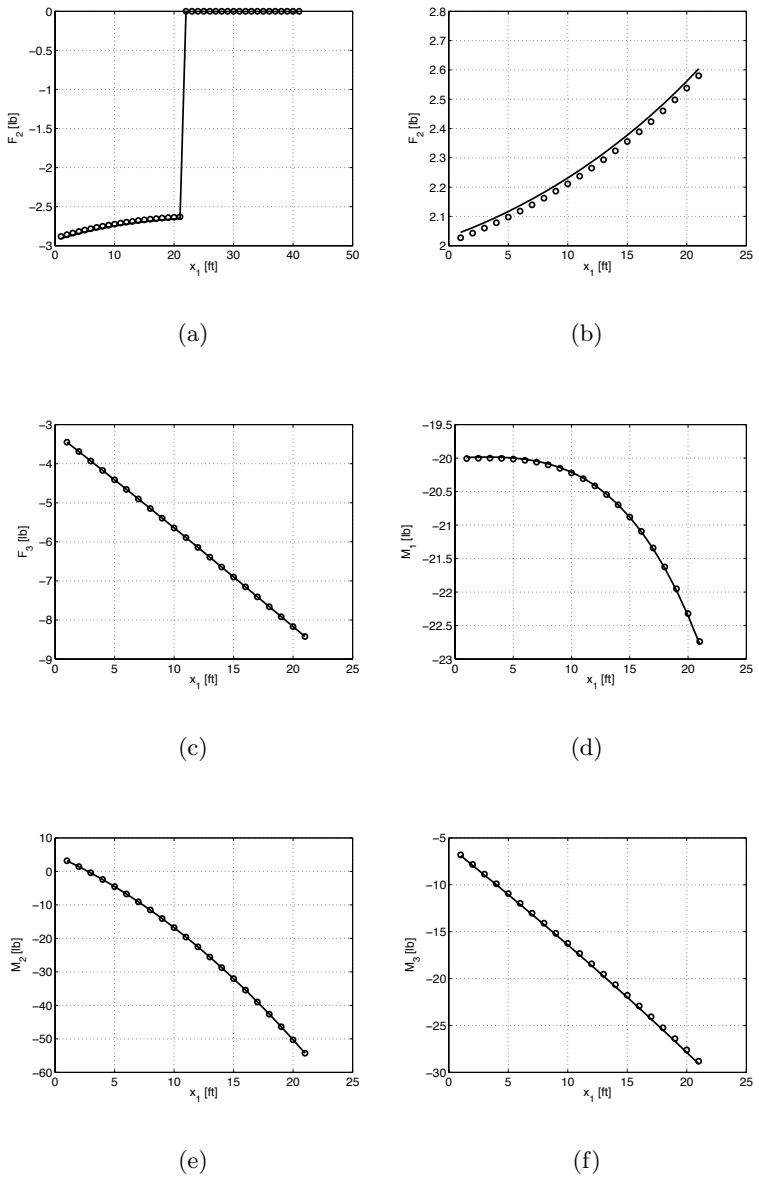

Figure 37: Force (a – c) and moment (d – f) distributions in back wing

Table 9: Aerodynamic properties

c_{l_0}	0
c_{l_α}	2π
c_{d_0}	0.01
c_{m_0}	0.025
c_{m_α}	-0.25
Velocity	10 ft/sec
Number of steps	500

4.3 Example: Instability Under Follower Force

In this section the effect of loading the front wing with a follower force in the chordwise direction is studied (resembling the thrust force of an engine). Figure 39 shows the configuration and Table 10 provides the structural properties for the problem at hand. Four forces are located at x_1=2.5, 7.5, 12.5 and 17.5 ft, and each has a value of F lb. Figure 40 shows the eigenvalues analysis of a clamped-free beam (i.e. only the front wing) under this loading. The first instability happens at F=40 lb. Figure 41 shows eigenvalue analysis of a joined-wing configuration (Fig. 39). For this case the sweep angle is 50° and the joint position is at $x_1 = 10$ ft. There is a fundamental difference between a single-load-path configuration (one beam) and a multiple-load-path configuration (joined-wing). The first instability for one beam, a static buckling type instability, occurs at F=40 lb. However, for a joined-wing configuration the first instability, which happens also to be at F=40 lb., is a dynamic instability. For this configuration a static instability occurs at F=74 lb., which is well beyond the first instability and, therefore, not of significance.

Table 10: Beam properties for configuration in Fig. 39, English units

Length of front wing	20 $[ft]$
Extensional stiffness	1.322×10^6 [lb]
Torsional stiffness	2.2138×10^3 [lb ft^2]
Out-of-plane bending stiffness	1.72146×10^3 [lb ft^2]
In-plane bending stiffness	1.09890×10^3 [lb ft^2]
Mass per unit length	0.012675 [slug/ft]

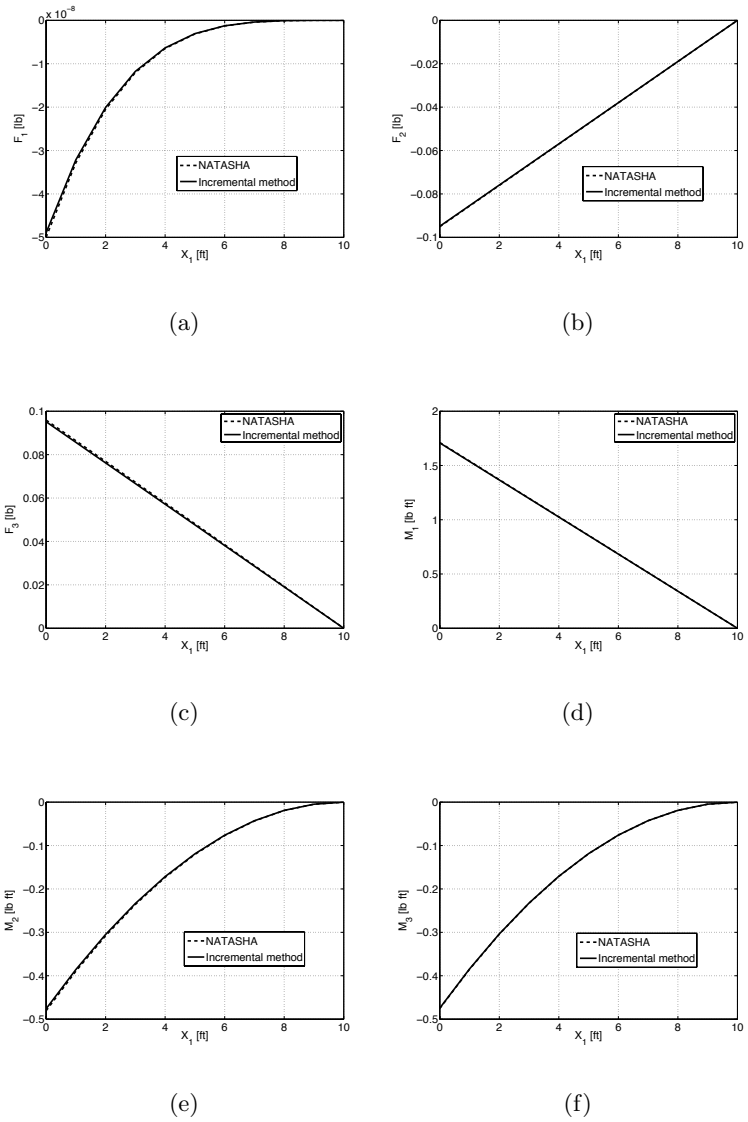

Figure 38: Force (a – c) and moment (d – f) distributions in clamped-free wing

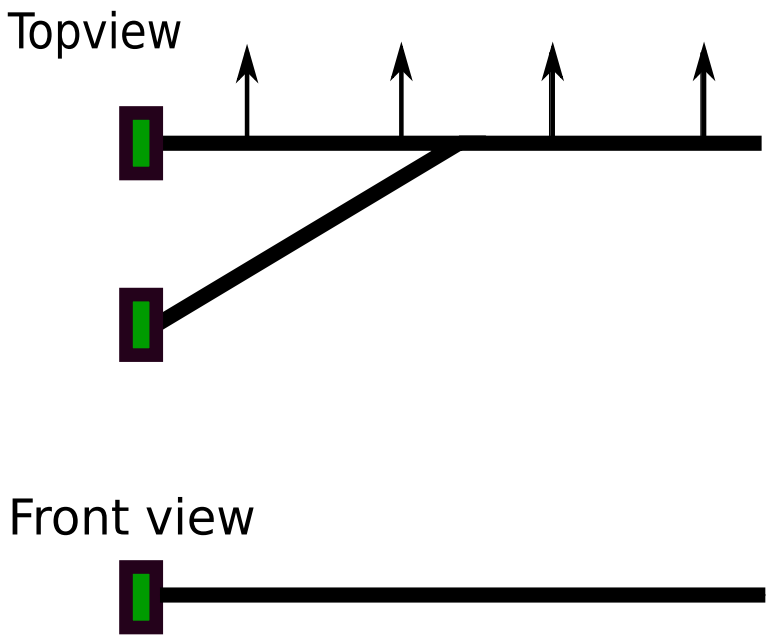

Figure 39: Sketch of configuration under thrust-like loading

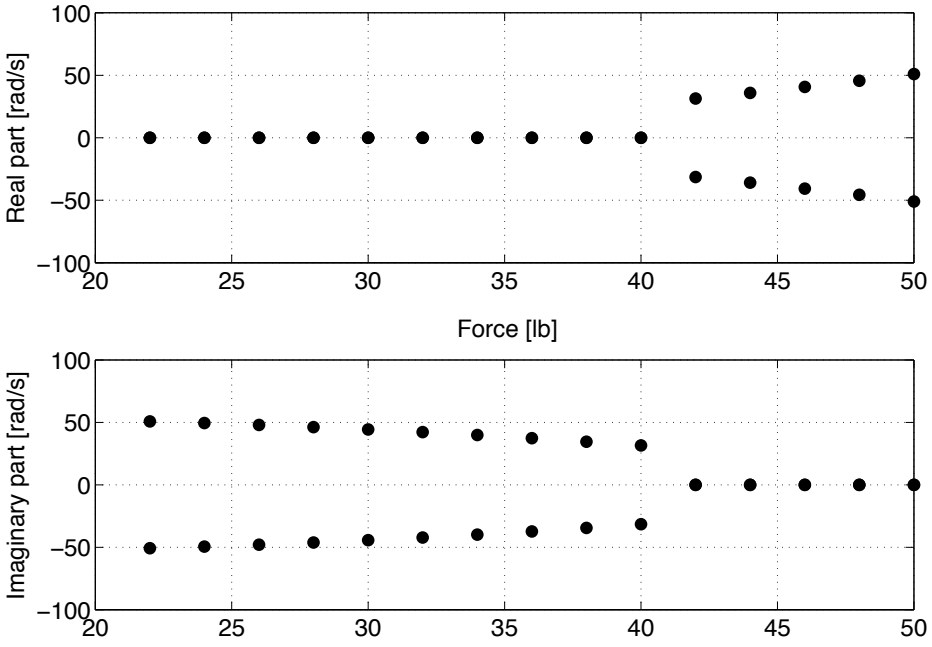

Figure 40: Eigenvalue analysis for one beam configuration

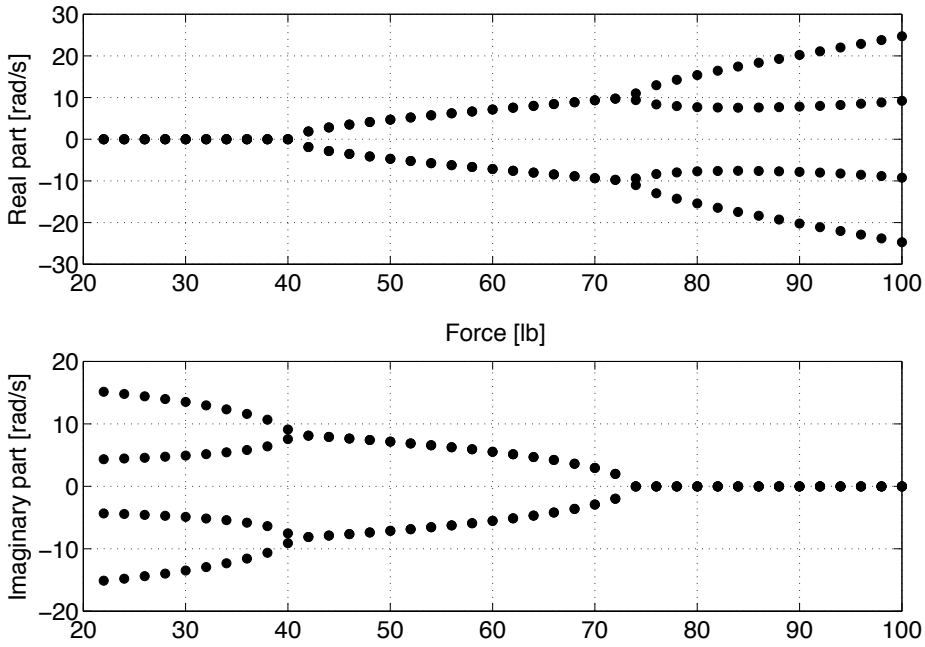

Figure 41: Eigenvalue analysis for joined-wing configuration

CHAPTER V

STABILITY AND DYNAMIC RESPONSE ANALYSIS OF ROTATING BLADES USING FULLY INTRINSIC EQUATIONS

This chapter is mostly adopted from Ref. [58], with the authors' permission.

As part of an ongoing investigation into potential advantages of fully intrinsic formulations, this chapter presents application of these equations in the modeling of rotor blades, in particular the modeling of hingeless and bearingless rotor configurations. Results obtained are presented and compared with those obtained from DYMORE for verification purposes.

5.1 Rotor Blade Configurations

This chapter includes a formulation and numerical results for realistic helicopter rotor blades. This formulation is based on fully intrinsic equations. Using this formulation a fast, user friendly computer program has been developed. Such a computer program is useful in preliminary design and optimization, in addition to stability analysis. Figure 42 shows topology of the simplest possible rotating blade. This configuration is a single-load-path blade. In this configuration the root of the blade is attached rigidly to the hub. A more realistic single-load-path configuration is shown in Fig. 43. In this configuration blade is attached to the hub through a sequence of hinges. Each hinge in this case is a revolute joint, which can be a flap, lead-lag or pitch hinge. This configuration is the simplest way of modeling an articulated blade. Figures 44 and 45 show blades with multiple-load paths, which are more realistic than those with single-load paths. These configurations include two bearings (inboard and outboard), which are both modeled as flexible joints. Designers can model different types of bearings by changing stiffness in the various directions. For example, the inboard bearing can model a revolute joint in the flap direction by having stiff springs in all directions except for rotation about a hinge in the flapping direction. In the bearingless configuration, the end of the inboard bearing attaches to the flexbeam, whereas in the hingeless configuration, the end of this bearing attaches to the hub through a rigid connection.

Figure 42: Schematic of blade with single-load path

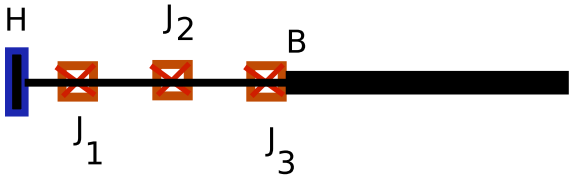

Figure 43: Schematic of blade with single-load path using a sequence of revolute joints

5.2 Formulation

The fully intrinsic equations are used to model each configuration. These equations are a system of PDEs, so one needs enough boundary and initial conditions to solve them. Geometric boundary conditions are here prescribed on velocity and angular velocity variables instead of displacement and rotation. Imposing natural boundary conditions is quite easy with formulations in which force and moment are among primary variables. Flexible and revolute joints are modeled by introducing extra degrees of freedom (deformation associated with translational and rotational springs). Chapter 3 shows how one can eliminate these extra degrees of freedom and come up with fully intrinsic equations for the whole structure [57].

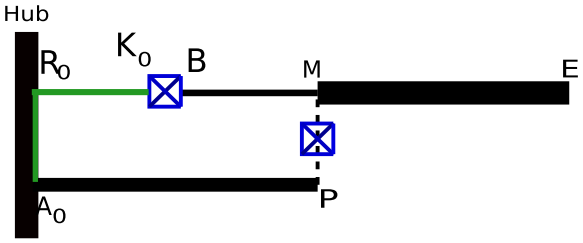

Figure 44: Schematic of hingeless blade with multiple-load paths

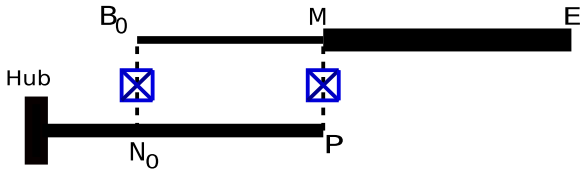

Figure 45: Schematic of bearingless blade with multiple-load paths

5.2.1 Single-load-path configuration

This configuration is consist of one beam. In case of a clamped-free beam, boundary conditions are simply

$$\left.\begin{aligned}\mathbf{V} &= 0\\ \mathbf{\Omega} &= 0\end{aligned}\right\} \text{at the root} \tag{63}$$

$$\left.\begin{aligned}\mathbf{F} &= 0\\ \mathbf{M} &= 0\end{aligned}\right\} \text{at the tip} \tag{64}$$

Boundary conditions for a single-load-path blade with three different hinges can be described through dynamics of hinges. Here l_1 is the offset of the first hinge (J_1) with respect to the hub; l_2 and l_3 are the offsets of the second and third hinges from the first and second hinges, respectively (Fig. 43). The offsets are assumed to be massless rigid bodies. This is a good assumption considering the fact that in the systems being modeled the offsets are much smaller than the blade length.

Frame H is attached to the hub with $\mathbf{h}_1$ along the first offset, frame D is attached to the first joint (J_1) with $\mathbf{d}_1$ along l_2 and frame F is attached to J_2 with $\mathbf{f}_1$ along l_3. The deformed beam cross-sectional frame of reference at root of the blade ($x_1 = 0$) is attached to J_3. For simplicity, this frame is called B here. There is a rotational spring associated with each joint: Joint J_1 is a revolute joint with a rotational degree of freedom θ_1 about axis $\mathbf{d}_m$; J_2 is a revolute joint with a rotational degree of freedom θ_2 about axis $\mathbf{f}_n$; and J_3 is a revolute joint with a rotational degree of freedom θ_3 about axis $\mathbf{B}_q$, where m, n and q can be any distinct combination of 1, 2 and 3. Boundary conditions on velocity and angular velocity at the root of the blade are

$$\left.\begin{aligned}\mathbf{V} - \mathbf{V}^* &= 0\\ \mathbf{\Omega} - \mathbf{\Omega}^* &= 0\end{aligned}\right\} \text{at the root} \tag{65}$$

$$
\begin{aligned}
\boldsymbol{\Omega}^* &= \dot{\theta}_1 \mathbf{d}_m + \dot{\theta}_2 \mathbf{f}_n + \dot{\theta}_3 \mathbf{B}_q + \boldsymbol{\Omega}_{\text{hub}} \\
\mathbf{V}^* &= l_1 \boldsymbol{\Omega}_{\text{hub}} \times \mathbf{h}_1 \\
&+ l_2(\boldsymbol{\Omega}_{\text{hub}} + \dot{\theta}_1 \mathbf{d}_m) \times \mathbf{h}_1 \\
&+ l_3(\boldsymbol{\Omega}_{\text{hub}} + \dot{\theta}_1 \mathbf{d}_m + \dot{\theta}_2 \mathbf{f}_n) \times \mathbf{f}_1 \\
m, n, q &= 1, 2, 3
\end{aligned}
\tag{66}
$$

Three extra variables are introduced (θ_1, θ_2 and θ_3); hence, three extra equations are needed. These equations are the moment equilibrium about each hinge:

$$
\begin{aligned}
K_1 \theta_1 &= \mathbf{d}_m \cdot \mathbf{M} + l_2(\mathbf{d}_m \times \mathbf{h}_1) \cdot \mathbf{F} + l_3(\mathbf{f}_n \times \mathbf{f}_1) \cdot \mathbf{F} \\
K_2 \theta_2 &= \mathbf{f}_n \cdot \mathbf{M} + l_3(\mathbf{f}_n \times \mathbf{f}_1) \cdot \mathbf{F} \\
K_3 \theta_3 &= \mathbf{B}_q \cdot \mathbf{M}
\end{aligned}
\tag{67}
$$

5.2.2 Dual-load-path configuration

Hingeless and bearingless configurations (Figs. 44 and 45) are dual-load-path configurations, and two beams are used to model them. For each beam an appropriate number of boundary conditions is needed. In addition one should model the inboard and outboard bearings. Figures 46 and 47 show different frames of reference that are used in modeling the inboard flexible joint in hingeless and bearingless configurations. The inboard bearing consists of three translational springs and three rotational springs. Pitch-link dynamics has not yet been incorporated in this model; instead, a pitch-control input angle is modeled as Θ_0.

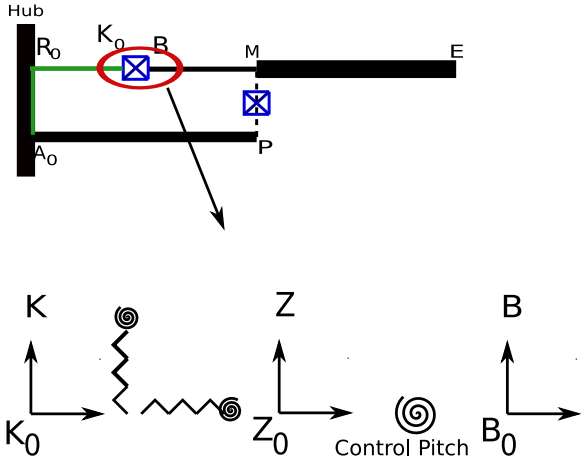

Figure 46: Inboard bearing in the hingeless configuration

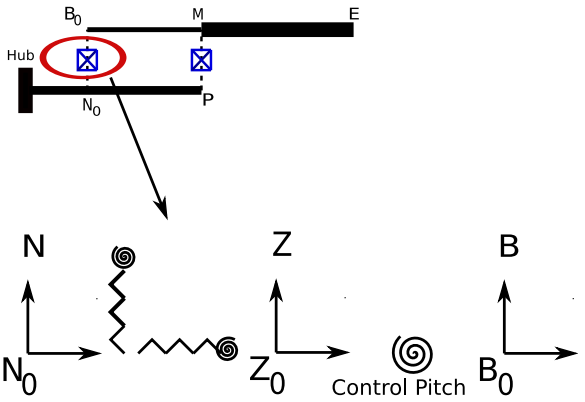

Figure 47: Inboard bearing in the bearingless configuration

5.2.2.1 Hingeless configuration

Boundary conditions for the lower beam (yoke) are

$$\left.\begin{aligned}\mathbf{V}-\mathbf{V}_{\text{hub}}&=0\\ \boldsymbol{\Omega}-\boldsymbol{\Omega}_{\text{hub}}&=0\end{aligned}\right\}\text{ at the root} \tag{68}$$

and

$$\left.\begin{aligned}\mathbf{F}-\mathbf{F}_{\text{joint}}&=0\\ \mathbf{M}-\mathbf{M}_{\text{joint}}&=0\end{aligned}\right\}\text{ at the tip} \tag{69}$$

The second beam consists of a spindle and blade (upper beam in Fig. 44). Boundary conditions for this beam are

$$\left.\begin{aligned}\mathbf{V}-\mathbf{V}^{*}&=0\\ \boldsymbol{\Omega}-\boldsymbol{\Omega}^{*}&=0\end{aligned}\right\}\text{ at the root} \tag{70}$$

$$\begin{aligned}\mathbf{V}^{*}&=|\mathbf{r}_{R_0K_0}|\boldsymbol{\Omega}_{\text{hub}}\times\mathbf{h}_1+\dot{\mathbf{U}}+\boldsymbol{\Omega}_{\text{hub}}\times\mathbf{U}\\ \boldsymbol{\Omega}^{*}&=\boldsymbol{\Omega}_{\text{hub}}+\dot{\boldsymbol{\Theta}}\end{aligned} \tag{71}$$

$$\left.\begin{aligned}\mathbf{F}&=0\\ \mathbf{M}&=0\end{aligned}\right\}\text{ at the tip} \tag{72}$$

Extra equations associated with the inboard bearing can be derived with either a Newton-Euler method or an energy approach. The resulting equations are

$$\begin{aligned}\mathbf{F}_{\mathbf{B_0}}-\underline{\mathbf{K}}_{l_{\text{in}}}\mathbf{U}-\underline{\mathbf{C}}_{l_{\text{in}}}\dot{\mathbf{U}}&=0\\ \mathbf{M}_{\mathbf{B_0}}-\underline{\mathbf{K}}_{r_{\text{in}}}\boldsymbol{\Theta}-\underline{\mathbf{C}}_{r_{\text{in}}}\dot{\boldsymbol{\Theta}}&=0\end{aligned} \tag{73}$$

These two equations are for the applied force and moment from the joint at the first node of the upper beam (spindle).

5.2.2.2 Bearingless configuration

Boundary conditions for the lower beam (flexbeam) are

$$\left.\begin{aligned}\mathbf{V}-\mathbf{V}_{\text{hub}}&=0\\ \boldsymbol{\Omega}-\boldsymbol{\Omega}_{\text{hub}}&=0\end{aligned}\right\}\text{at the root} \tag{74}$$

$$\left.\begin{aligned}\mathbf{F}-\mathbf{F}_{\text{joint}}&=0\\ \mathbf{M}-\mathbf{M}_{\text{joint}}&=0\end{aligned}\right\}\text{at the root} \tag{75}$$

The second beam consists of a cuff and a blade (upper beam in Fig. 44). Boundary conditions for this beam are

$$\left.\begin{aligned}\mathbf{V}-\mathbf{V}^{*}&=0\\ \boldsymbol{\Omega}-\boldsymbol{\Omega}^{*}&=0\end{aligned}\right\}\text{at the root} \tag{76}$$

$$\begin{aligned}\mathbf{V}^{*}&=\mathbf{V}_{\mathbf{N_0}}+\dot{\mathbf{U}}+\boldsymbol{\Omega}_N\times\mathbf{U}+\dot{\boldsymbol{\Theta}}\times\mathbf{U}\\ \boldsymbol{\Omega}^{*}&=\boldsymbol{\Omega}_N+\dot{\boldsymbol{\Theta}}\end{aligned} \tag{77}$$

$$\left.\begin{aligned}\mathbf{F}&=0\\ \mathbf{M}&=0\end{aligned}\right\}\text{at the tip} \tag{78}$$

Extra equations associated with the inboard bearing can be derived with either a Newton-Euler method or an energy method. The resulting equations are

$$\begin{aligned}\mathbf{F}_{\mathbf{B_0}}-\underline{\mathbf{K}}_{l_{\text{in}}}\mathbf{U}-\underline{\mathbf{C}}_{l_{\text{in}}}\dot{\mathbf{U}}&=0\\ \mathbf{M}_{\mathbf{B_0}}-\underline{\mathbf{K}}_{r_{\text{in}}}\boldsymbol{\Theta}-\underline{\mathbf{C}}_{r_{\text{in}}}\dot{\boldsymbol{\Theta}}&=0\end{aligned} \tag{79}$$

These two equations are for the applied force and moment from the joint at the first node of the upper beam (cuff). In this configuration, unlike the hingeless configuration, the cuff is attached to the flexbeam with both inboard and outboard bearings; therefore, there are applied forces and moments on the connection node of the inboard bearing and flexbeam, given by

$$\begin{aligned}\mathbf{F}_J&=\mathbf{F}_{\mathbf{B_0}}\\ \mathbf{M}_J&=|\mathbf{r}_{R_0K_0}|\mathbf{h}_1\times\mathbf{F}_{\mathbf{B_0}}+\mathbf{M}_{\mathbf{B_0}}\end{aligned} \tag{80}$$

5.2.2.3 Outboard bearing

Figures 48 and 49 show the components of the outboard bearing in the hingeless and bearingless configurations. Displacement and orientation of nodes M and P can be calculated from Eqs. (5) and (6). Hence, nodal forces and moments at nodes M and P in the local frame of reference may be computed as

$$\begin{aligned} f^M_{\text{nodal}} &= K_{l_{MP}} C^{BI}_M \Delta U \\ f^P_{\text{nodal}} &= K_{l_{MP}} C^{BI}_P \Delta U \\ m^M_{\text{nodal}} &= K_{r_{MP}} C^{BI}_M \Delta\Theta \\ m^P_{\text{nodal}} &= K_{r_{MP}} C^{BI}_P \Delta\Theta \end{aligned} \tag{81}$$

where ΔU is the relative displacement of nodes M and P in the inertial frame, $K_{l_{MP}}$ is a 3×3 diagonal matrix the elements of which are translational spring stiffness in the outboard bearing, C^{BI}_M is the direction cosine matrix of the deformed beam cross-sectional frame at node M, $K_{r_{MP}}$ is a 3×3 diagonal matrix the elements of which are rotational spring stiffness in the outboard bearing, and $\Delta\Theta$ is the relative rotation which can be calculated from

$$\widetilde{\Delta\Theta} = \frac{2(C^{MP^T} - C^{MP})}{1 + \text{Trace}(C^{MP})} \tag{82}$$

with C^{MP} being the direction cosine matrix of the B frame (deformed beam cross-sectional frame) at node P with respect to B frame at node M, viz.,

$$C^{MP} = C^{BI}_P C^{IB}_M \tag{83}$$

5.2.3 Flap or lead-lag hub connection

In order to consider a more realistic attachment of the blade to the hub, one can model the hub attachment as a flap or lead-lag hinge with a rotational spring instead of a clamped boundary condition. In this case boundary conditions for the flexbeam root are

$$\begin{aligned} &\mathbf{V} - \mathbf{V}_{\text{hub}} = 0 \\ &\mathbf{\Omega} - \mathbf{\Omega}_{\text{hub}} - \dot{\beta}\mathbf{h}_m = 0 \\ &m = 2, 3 \end{aligned} \tag{84}$$

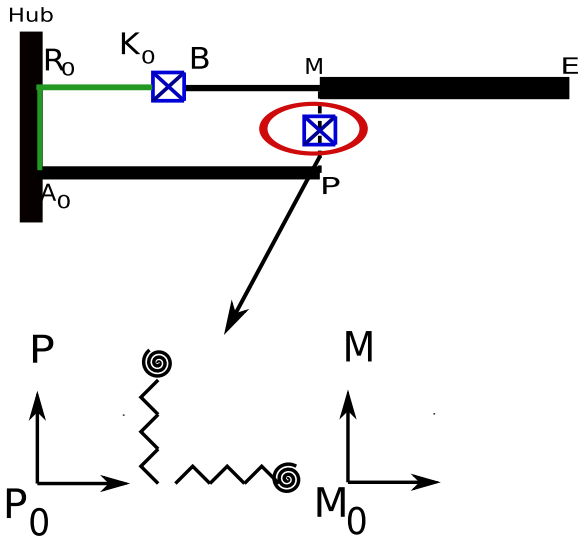

Figure 48: Hingeless configuration, outboard bearing

m is 2 for a flap hinge and 3 for a lead-lag hinge. β is an extra degree of freedom associated with the rotational deflection of flap (or lead-lag) hinge. One more extra equations is needed for this configuration:

$$\left.\mathbf{M}\cdot\mathbf{h}_m = k_\beta\beta\right\} \text{ at the root} \tag{85}$$

5.3 Solution Procedure

In this work three different types of solutions for each configuration are studied:

- *Steady-state solution for rotating blades in hover*: The fully intrinsic equations can be specialized for a steady-state solution by dropping all time derivatives. Since the B frame (the deformed beam cross-sectional frame of reference) is a rotating frame, the steady-state equations are independent of the harmonics of rotor angular speed. Hence, the steady-state equations are a system of time-independent, nonlinear ODEs in space. A finite element or a simple finite difference discretization may be used to obtain a system of nonlinear algebraic equations. The Newton-Raphson method is then used to solve this set of equations and find the steady-state solution.

- *Constant-coefficient eigenvalue analysis for studying stability of rotating blade in hover*: The nonlinear fully intrinsic equations can be linearized about a steady-state solution. In hover these equations lead to a constant-coefficient, generalized eigenvalue problem.

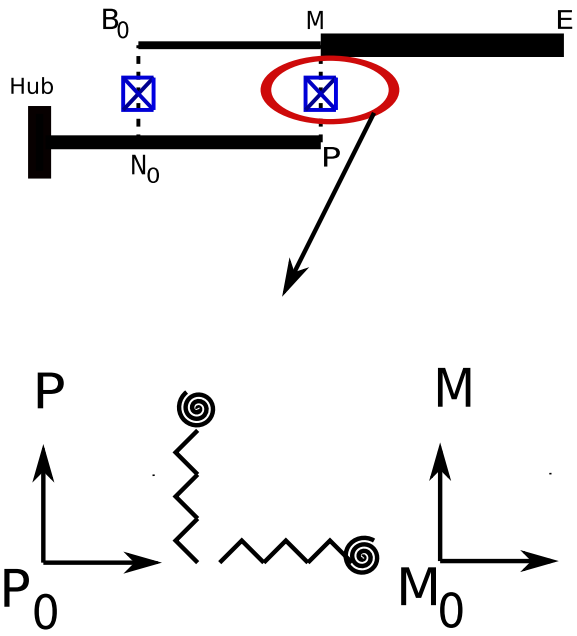

Figure 49: Bearingless configuration, outboard bearing

With an appropriate aerodynamics model the resulting eigenvalues may be then used to assess the stability of the rotor about the blade steady-state solution.

- *Dynamic response of rotating blade*: The nonlinear fully intrinsic equations may be discretized in both space and time and marched to a given time from specified initial conditions. This way a fully nonlinear dynamic solution can be obtained.

5.4 Numerical Results

In this section the implementation of these formulations are verified against DYMORE [1] results. Considerable verification has been done using textbook problems as well. In the this section two examples are presented. Example one shows a typical section flutter analysis, and example two shows static deflection of a hinged-free beam under its own weight in the nonlinear regime.

5.4.1 Ex. 1: typical section flutter analysis

In this example the hingeless configuration is used to model typical section flutter. For this purpose both beams of the hingeless configuration are rigid. All spring constants for the outboard bearing are zero. All spring constants for the inboard bearing are very large

except for spring stiffness in the pitch and plunge directions. The 2D induced flow theory of Peters et al. [48] and strip theory are used to form the aerodynamic model [44]. For this textbook case [35] the mass ratio μ is 2; the ratio of plunge frequency to pitch frequency σ is 0.4; the dimensionless radius of gyration r is 0.49; and the elastic axis is behind the aerodynamic center a distance of 0.1 half-chord. The pitch stiffness of the inboard bearing is 10,000.[1] Figure 50 shows the current results along with virtually identical results from the solution found in Ref. [35]. It should be noted that these results are dimensional.

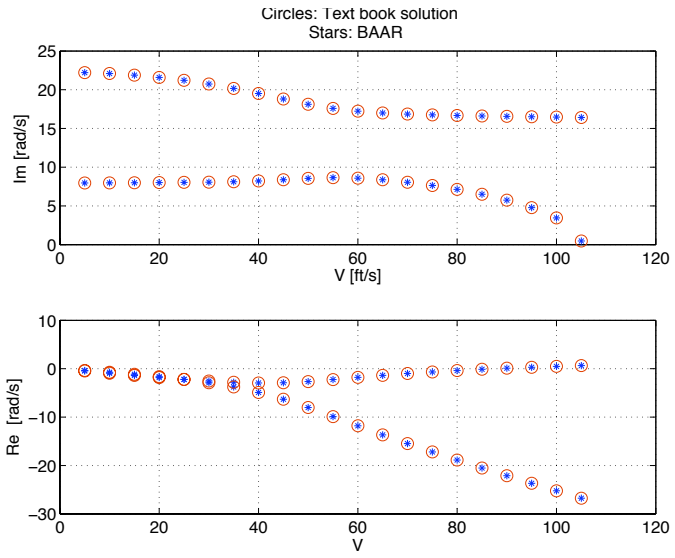

Figure 50: Classical flutter analysis using hingeless configuration

5.4.2 Ex. 2: Static deflection of a beam under its own weight

The static deflection of a beam under its own weight is calculated using the same formulation as the one used for the single-load-path configuration (Fig. 43). In this example all the offsets are zero, and the model is based on two very stiff springs about the rotational hinges in the pitch and lead-lag directions, and a spring of moderately large stiffness about the flap direction. These results are compared with a numerical solution of the same equations except that the rotational spring is modeled in intrinsic form. For this purpose two more variables (i_1, i_2) are introduced, where $i = \lfloor i_1 \quad i_2 \quad i_3 \rfloor^T$ is a column matrix of the measure

[1] Note that all dimensional quantities used in this paper may be regarded as being expressed in any internally consistent system of units (e.g. pounds, feet, slugs, seconds or Newtons, meters, kilograms, seconds).

numbers of a unit vector in the direction of gravity expressed in the B basis [44]. Thus,

$$\begin{aligned}
&F_1' + \mu g i_1 + \frac{F_3 M_2}{EI} = 0 \\
&F_3' - \mu g i_3 + \frac{F_1 M_2}{EI} = 0 \\
&M_2' - \left(1 + \frac{F_1}{EA}\right) F_3 = 0 \\
&i_1' + \frac{i_3 M_2}{EI} = 0 \\
&i_3' - \frac{i_1 M_2}{EI} = 0
\end{aligned} \tag{86}$$

An intrinsic form of the boundary conditions is

$$\begin{aligned}
&F_1(L) = 0 \\
&F_3(L) = 0 \\
&M_2(L) = 0 \\
&i_1(0) - \sin\left[\frac{M_2(0)}{k}\right] = 0 \\
&i_3(0) + \cos\left[\frac{M_2(0)}{k}\right] = 0
\end{aligned} \tag{87}$$

Table 11 shows the properties of this test case, and Fig. 51 shows the results.

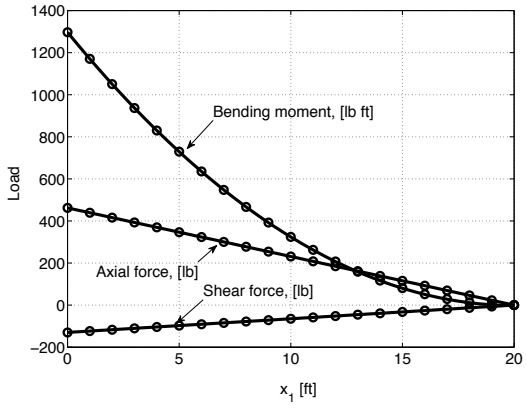

Figure 51: Spring restrained pinned-free beam under its own weight

5.5 Verification Against DYMORE

In this section, the implementation of the fully intrinsic formulation is verified against DYMORE for each configuration.

Table 11: Properties, English unit system

Mass per unit of length	0.746 $[slug/ft]$
Bending stiffness	23.65×10^6 [lb ft^2]
Axial stiffness	10^8 [lb]
Rotational spring stiffness	1000.0 [lb ft/rad]
Length	20.0 [ft]
Gravitational constant	32.174 [ft/s^2]

5.5.1 Single-load path

Structural properties for this case are the same as for the Goland wing [21]. Figure 52 shows the internal force and moment distributions along the beam axis. For these results the beam is loaded by its own weight, and the hub angular speed is 11 rad/s. 20 elements are used for both DYMORE and the fully intrinsic equation model. Table 12 shows natural frequencies of the same configuration when the center of mass offset is zero. Recall that DYMORE elements are third-order elements, while the code based on fully intrinsic equations uses first-order elements.

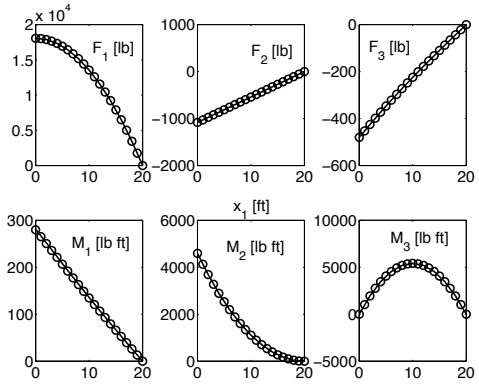

Figure 52: Steady-state response of a clamped-free beam under its own weight

Figure 53 shows results obtained for the flapping natural frequencies of a rotating clamped-free beam using fully intrinsic equations, which are compared with those from Ref. [30]. Fig. 54 shows results obtained for the flapping natural frequencies of a rotating pinned-free beam, which are compared versus the exact solution [64].

Dynamic response of a clamped-free blade under a harmonic load at the tip is studied.

Table 12: Natural frequencies [rad/s] of clamped-free beam

DYMORE	Fully Intrinsic	Fully Intrinsic	Fully Intrinsic
20 elements	20 elements	40 elements	60 elements
49.055	49.093	49.065	49.059
87.017	87.062	87.028	87.022
261.052	262.266	261.354	261.186
292.478	295.093	293.128	292.767
435.087	440.765	436.490	435.709
476.875	477.192	476.954	476.910
609.119	624.942	612.986	610.831
764.058	781.328	768.316	765.945

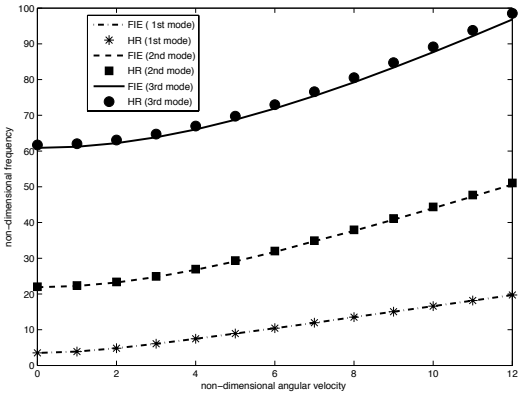

Figure 53: Natural frequencies $\omega\sqrt{\frac{mL^4}{EI}}$ of a clamped-free rotating beam; lines are results obtained from the fully intrinsic equations, and symbols are from Ref. [30]

The beam has the properties of the Goland wing [21], but with zero offset of the center of mass. The applied harmonic force at the tip is $10\mathbf{B_3}\sin(2\pi t/5)$. Figure 55 shows the force and bending moment at the root of the blade, where they have their maximum values, over one period.

5.5.2 Dual-load-path, hingeless configuration

The hingeless configuration (Fig. 44) is modeled in DYMORE and with fully intrinsic equations. The steady-state response, natural frequencies and dynamic response are compared with DYMORE results. Table 13 shows properties of this test case.

Figure 56 shows the force and moment distributions in the blade loaded by its own weight and the effect of rotation. Table 14 shows some of the natural frequencies versus

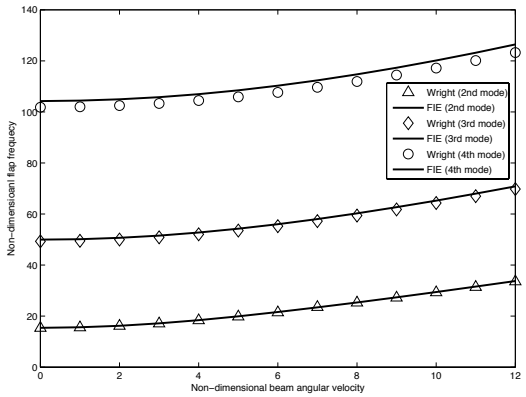

Figure 54: Natural frequencies $\omega\sqrt{\frac{mL^4}{EI}}$ of a pinned-free rotating beam; lines are results obtained from fully intrinsic equations, and symbols are from Ref. [64]

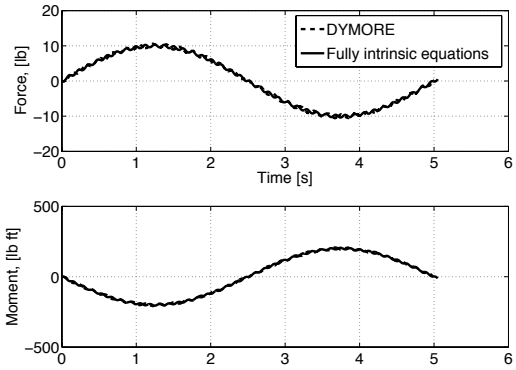

Figure 55: Dynamic response of a clamped-free beam

DYMORE's results. 22 first-order elements are used for the fully intrinsic solution, and the same number of third-order elements is used in DYMORE. The difference in the orders partially accounts for differences in the results.

Dynamic response of the hingeless configuration with properties given in Table 13 is studied for the case of a harmonic load applied at the blade tip. The applied harmonic force at the tip of the beam is $10\mathbf{B_3}\sin(2\pi t/5)$. Figure 57 shows force and moment at the root of the blade over one period.

Table 13: Properties for hingeless configuration, English unit system. Unit for translational spring is [lb/ft] and unit for rotational spring is [lb ft/rad].

Rigid connection length	2.0 [ft]
Spindle length	2.0 [ft]
Yoke length	4.0 [ft]
Blade length	16.0 [ft]
Axial stiffness	10^8 [lb]
Out of plane	
Bending stiffness	23.65×10^6 [lb ft^2]
In-plane bending stiffness	30.0×10^7 [lb ft^2]
Mass per unit of length	0.5 [slug/ft]
Mass moment of inertia per unit of length	0.002 [ft^3]
Inboard spring stiffness (all)	10^7
Outboard translational spring stiffness (all)	10^6
Outboard rotational spring stiffness (all)	100.0
Gravitational constant	32.174 [ft/s^2]
Hub angular velocity	10 [rad/s]
Harmonic load	$10\mathbf{B_3}\sin(2\pi t/5)$ [lb]

5.5.3 Dual-load-path, bearingless configuration

The bearingless configuration (Fig. 45) is modeled via DYMORE and fully intrinsic equations. Results obtained from the current approach for steady-state response, natural frequencies and dynamic response are compared with those obtained from DYMORE. Table 15 shows properties of this test case.

Figure 58 shows force and moment distributions in the blade loaded by its own weight and the effect of rotation. Table 16 shows the natural frequencies versus those obtained from

Table 14: Natural frequencies [rad/s] of hingeless configuration

DYMORE	Fully Intrinsic formulation	Percentage difference
6.13	6.13	0
42.41	42.60	0.4
325.66	327.96	0.7
354.04	357.06	0.8
358.90	362.37	0.9
623.49	629.54	0.9

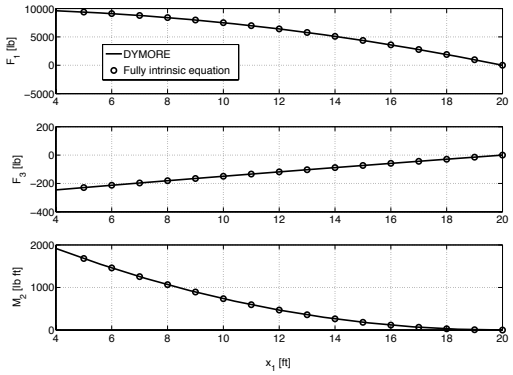

Figure 56: Steady-state solution of hingeless configuration

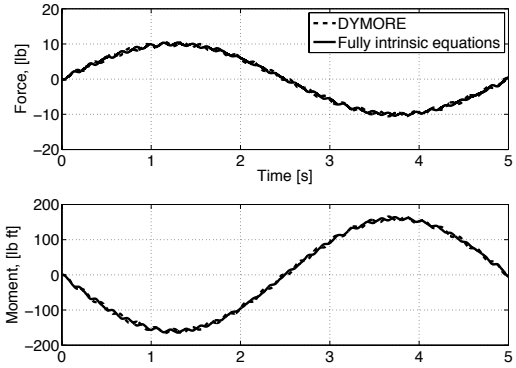

Figure 57: Dynamic response of hingeless configuration

DYMORE. 22 first-order elements are used for the fully intrinsic solution, and the same number of (third-order) elements is used in DYMORE. The difference in orders partially accounts for the slightly different results obtained for frequencies of the higher modes.

Dynamic response of the hingeless configuration from a harmonic load applied at the blade tip is studied using the properties given in Table 15 . The applied harmonic force at the tip of the beam is $10\mathbf{B_3}\sin(2\pi t/5)$. Figure 59 shows the force and moment at the root of the blade over one period.

5.5.4 Flap or lead-lag hub connection

Figure 60 shows shear force and bending moment distributions for the bearingless configuration having a spring-restrained flapping hinge attached to the hub and with a spring

Table 15: Properties for bearingless configuration, English unit system, unit for translational spring is [lb/ft] and unit for rotational spring is [lb ft/rad].

Cuff length	2.0 [ft]
Flexbeam length	4.0 [ft]
Blade length	16.0 [ft]
Axial stiffness	10^7
Out of plane	
bending stiffness	23.65×10^6 [lb ft^2]
In-plane bending stiffness	30.0×10^7 [lb ft^2]
Mass per unit of length	0.5 [slug/ft]
Mass moment of inertia	0.002 [ft^3]
Inboard spring stiffness	
spring stiffness (all)	10^6
Outboard translational	
Outboard rotational	
spring stiffness (all)	100.0
Gravitational constant	32.174 [ft/s^2]
Hub angular velocity	10 [rad/s]
Harmonic load	$10\mathbf{B_3}\sin(2\pi t/5)$ [ft]

constant of 1000. This configuration is loaded under its own weight and the effect of rotation. Table 17 shows the natural frequencies for this case.

Figure 61 shows shear force and bending moment distributions for the bearingless configuration for the same case except with a spring-restrained lead-lag hinge instead of flapping hinge. Table 18 shows the natural frequencies for this case. Figure 62 and 63 shows change of natural frequencies with the change of rotational spring stiffness at the hub for flap hinge and lead-lag hinge, respectively.

Table 16: Natural frequencies [rad/s] of hingeless configuration

DYMORE	Fully Intrinsic formulation	Percentage difference
6.142	6.142	0
61.022	61.364	0.5
373.184	375.034	0.5
1013.02	1022.81	0.9
1024.41	1037.99	1.3
1126.33	1132.53	0.5
1961.17	1973.21	0.6

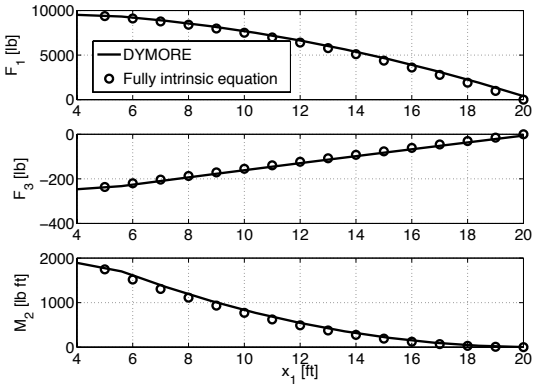

Figure 58: Steady-state solution of bearingless configuration

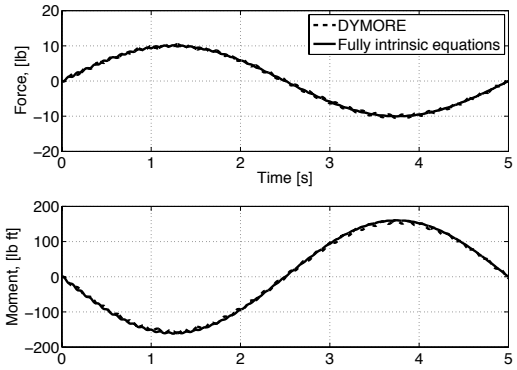

Figure 59: Dynamic response of hingeless configuration

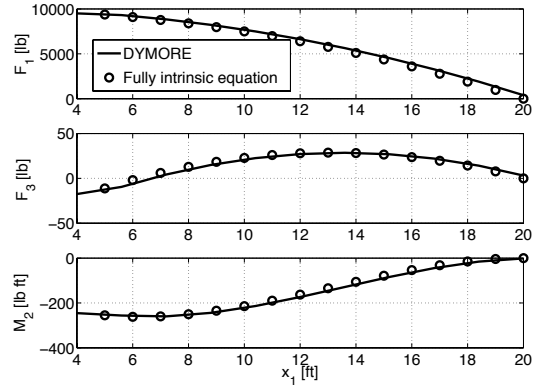

Figure 60: Force and moment distribution in bearingless configuration with flap connection to the hub

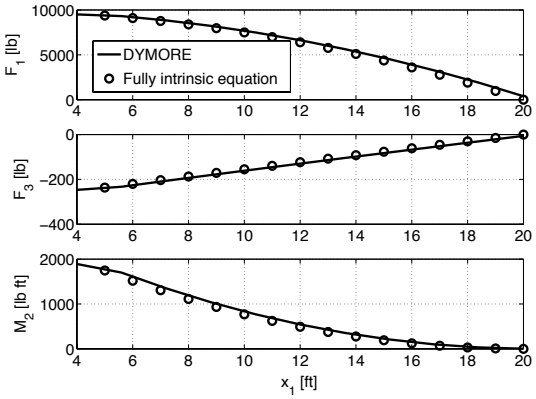

Figure 61: Force and moment distribution in bearingless configuration with lead-lag connection to the hub

Table 17: Natural frequencies [rad/s] of bearingless configuration with flap connection to the hub

DYMORE	Fully Intrinsic formulation
6.141	6.131
10.034	10.051
260.196	261.595
809.946	822.447
1012.90	1022.66

Table 18: Natural frequencies of bearingless [rad/s] configuration with lead-lag connection to the hub

DYMORE	Fully Intrinsic formulation
0.855	0.850
2.890	28.950
61.022	61.367
373.309	375.021
1012.87	1023.10

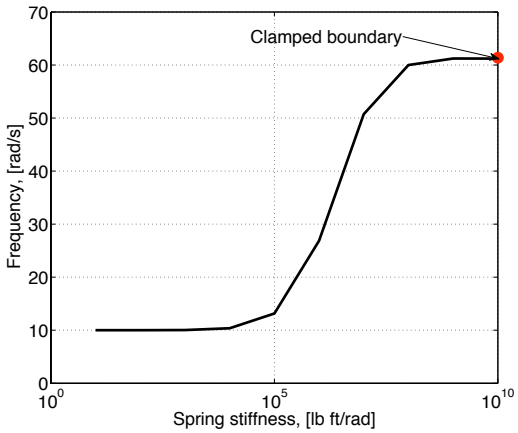

Figure 62: Change of natural frequency [rad/s] with the change of spring stiffness in bearingless configuration with flap connection to the hub

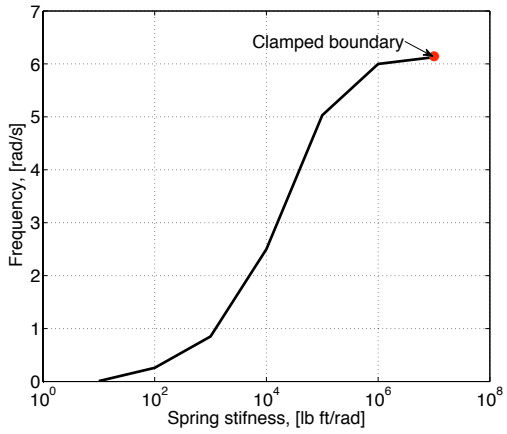

Figure 63: Change of natural frequency [rad/s] with the change of spring stiffness in bearingless configuration with lead-lag connection to the hub

CHAPTER VI

CONCLUSION AND FUTURE WORK

6.1 Conclusion

The fully intrinsic equations for beams comprise a relatively new set of equations for nonlinear modeling of structures comprised of beams. These equations are geometrically exact and constitute a closed set of equations even though they include neither displacement nor rotation variables. They do not suffer from the singularities and infinite-degree nonlinearities normally associated with finite rotation variables and they have maximum degree of nonlinearity equal to two. .

Given certain advantages of the fully intrinsic equations, it is of interest to explore how they can be used for problems with certain boundary conditions, which as has been shown herein can be a challenge. This work takes a first look at these challenges, most of which occur in modeling statically indeterminate structures. Different methods are introduced to overcome these obstacles in static equilibrium, steady-state motion and linearized dynamic analyses. One of the purposes of this work is to help researchers decide whether or not fully intrinsic equations are suitable for solving a specific problem. By presenting a set of examples, a path has now been cleared for wider use of the fully intrinsic equations in future research. Beams with one end free (or with prescribed values for moment and force) can be solved easily using the fully intrinsic equations. It also is shown that the fully intrinsic equations are especially well-suited for modeling rotating beams.

A new way of analyzing statically indeterminate structures (with multiple load paths such as used in joined-wing aircraft), is introduced. The formulation is based on the fully intrinsic equations of motion and kinematics and introduces neither singularities nor infinite-degree nonlinearities caused by finite rotation. Instead it makes use of an incremental form of the governing equations of motion and kinematics, augmented by an incremental equation for change in displacement and orientation. This formulation leads to solution of a linear system of equations at each incremental loading step, thus avoiding the numerical difficulties

associated with solving nonlinear systems of equations such as finding suitable initial guesses and achieving robust convergence. There is also no need to parameterize finite rotation with orientation angles, Rodrigues parameters, etc. Consequently, there are neither singularities nor infinite degree nonlinearities associated with finite rotation in the present formulation. The main advantageous features of the fully intrinsic equations are thus preserved. The method is verified and applied to a joined-wing structure. Results obtained indicate that the method is (a) capable by itself of obtaining the nonlinear static or steady motion solution for the static, dynamic or aeroelastic behavior of statically indeterminate structures and (b) capable of providing an accurate set of initial guesses as needed or desired for a Newton-Raphson solution of both statically determinate and indeterminate structures.

The nonlinear fully intrinsic equations are used in this work to study dynamic response of helicopter blades as well. This approach leads to a computationally efficient and user-friendly program that can be used in parametric studies as well as conceptual and preliminary design. While the program has nowhere near the capability of general-purpose, multi-flexible-body codes, such as DYMORE, it has the same level of accuracy for the cases that it is set up to handle, providing an accurate dynamic model with low overhead that can be used in conceptual design, preliminary design and optimization studies.

6.2 Future Work

Further research and development can be done along the following lines based on the studies that have done in this work.

- *Improvement of incremental method.* A mathematical proof of convergence for the incremental method is desirable. Also the non-orthogonality of update equation of direction cosine matrix may be addressed in future. The rotation update equation given in Refs. [53, 52] may be useful in addressing this deficiency of incremental method, presented in this work.

- *Aeroelastic analysis of blade.* Dynamic stall flutter is an important phenomena in helicopter aeroelasticity. The computational cost of such analysis is expensive. Using fully intrinsic equations minimizes the use of direction cosine matrix. This reduces the

computational cost significantly. Currently BAAR has the basic features for structural dynamics analysis of helicopter rotor blades. An appropriate aerodynamic model is needed to be coupled with fully intrinsic equations for an aerolestic analysis of helicopter blade. Among many wake models, dynamic inflow [49] is one of the suitable ones. The finite-state inflow model represents a 3D wake model for incompressible flow. The wake is assumed to be cylindrical for the hovering flight condition.

- *Aeroelastic analysis of helicopter rotor.* Helicopter rotors are made of several blades. Fully intrinsic equations can be used to study of helicopter rotor, based on the fundamental studies that are done in this research. The so-called Multi-Blade Coordinate (MBC) transformation has been performed on displacement-based equations before; however, this approach has not been applied to fully intrinsic equations. When the MBC is applied to the hovering flight condition, the dependence of the equations on the blade number disappears from the aeroelastic model, resulting in sets equations with constant coefficients. A similar manipulation can be performed on the perturbed inflow equations to get sets of equations governing collective, differential and cyclic modes, respectively, of finite-state inflow variables. Distinct sets of equations then are obtained for the perturbed motion of collective, differential and cyclic modes, respectively. For the forward-flight regime, dependency on the blade number and time-dependent coefficients remain in the aeroelastic model. However, the importance of the periodic-coefficient terms diminishes, making a constant-coefficient approximation feasible. A harmonic balance approach may be used to find the trim solution. This approach avoids time consuming time-integration trim solutions.

- *Analyze Limit Cycle Oscillation (LCO) for HALE and conventional aircraft.* The linear theory of stability, when applied to aeroelasticity problems, typically leads to a set of eigenvalues. It predicts that small disturbances of a system at an unstable equilibrium grow exponentially. As far as it goes, linear theory is correct; that is, small disturbances do grow exponentially, at least at first. However, one should not regard the results of linear theory to have any significance whatsoever regarding the

behavior of a system subjected to large disturbances, or after a long time elapses from an initial small disturbance. For example, according to linear theory the system will continuously go away from the unstable equilibrium to infinity (or material failure). This does not always comport with experimental evidence, and nonlinear analysis methodology has been developed to remedy this problem [45]. If a system has a nonlinear stiffening term, then in most occasions the amplitude of oscillations will grow until an LCO is reached. LCOs, though stable in the sense of Lyapunov, are not asymptotically stable. That is, although the final state is bounded, the system will not asymptotically approach its original equilibrium state as time grows. Moreover, LCOs are not necessarily a result of a linear instability. LCOs can be induced by certain disturbances, if sufficiently large, even when the given equilibrium state is stable. Basically, if the disturbances are not small, then the response cannot be predicted by theories that are linearized about a nonlinear steady-state solution. Depending on the amplitude of the LCO, the structure may or may not experience immediate failure. However, for an aircraft, LCOs pose significant problems in their own right. The vibration caused by LCOs causes fatigue, reducing the useful life of the structure. Thus, efficient prediction of LCOs is very important during design, especially for aircraft flying near the limits of the linear assumptions [45]. The basic time-marching capability of both NATASHA and BAAR can be improved to be able to capture LCOs.

REFERENCES

[1] Bauchau, O. A., Bottasso, C. L., and Nikishkov, Y. G., "Modeling rotorcraft dynamics with finite element multibody procedures," *Mathematical and Computer Modeling*, vol. 33, pp. 1113 – 1137, 2001.

[2] Blair, M. and Canfield, R. A., "A joined-wing structural weight modeling study," in *Proceedings of the 43rd Structures, Structural Dynamics, and Materials Conference, Denver, Colorado*, (Reston, Virginia), AIAA, April 22 – 25, 2002. Paper AIAA 2002-1337.

[3] Blair, M. and Canfield, R. A., "Joined-wing aeroelastic design with geometric nonlinearity," *Journal of Aircraft*, vol. 42, no. 4, pp. 832–848, 2005.

[4] Boston, J., Swenson, E., Kunz, D., Yu, W., and Blair, M., "Experiments with geometric non-linear coupling for analytical validation," in *Proceedings of the 51st Structures, Structural Dynamics, and Materials Conference, Orlando, Florida*, (Reston, Virginia), AIAA, April 12 – 15, 2010. Paper AIAA-2010-3018.

[5] Cesnik, C. E. S. and Hodges, D. H., "VABS: a new concept for composite rotor blade cross-sectional modeling," *Journal of the American Helicopter Society*, vol. 42, pp. 27 – 38, January 1997.

[6] Cesnik, C. E. S. and Su, W., "Nonlinear aeroelastic modeling and analysis of fully flexible aircraft," in *Proceedings of 46th Structures, Structural Dynamics and Materials Conference, Austin, Texas*, (Reston, Virginia), AIAA, April 18 – 21, 2005.

[7] Cesnik, C. and Brown, E., "Active warping control of a joined-wing airplane configuration," in *Proceedings of 44th Structures, Structural Dynamics, and Materials Conference, Norfolk, Virginia*, (Reston, Virginia), AIAA, April 7 – 10, 2003.

[8] Chang, C.-S. and Hodges, D. H., "Parametric studies on ground vibration test modeling for highly flexible aircraft," *Journal of Aircraft*, vol. 44, pp. 2049 – 2059, Nov.-Dec. 2007.

[9] Chang, C.-S. and Hodges, D. H., "Stability studies for curved beams," *Journal of Mechanics of Materials and Structures*, vol. 4, no. 7, pp. 1257 – 1270, 2009.

[10] Chang, C.-S. and Hodges, D. H., "Vibration characteristics of curved beams," *Journal of Mechanics of Materials and Structures*, vol. 4, no. 4, pp. 675 – 692, 2009.

[11] Chang, C.-S., Hodges, D. H., and Patil, M. J., "Flight dynamics of highly flexible aircraft," *Journal of Aircraft*, vol. 45, pp. 538 – 545, Mar.-Apr. 2008.

[12] de Andrade, D. and Peters, D. A., "Correlation of experimental flap-lag-torsion damping – a case study," *Mathematical and Computer Modelling*, vol. 19, no. 3/4, pp. 135 – 158, 1994.

[13] Demasi, L. and Livne, E., "Exploratory studies of joined wing aeroelasticity," in *Proceedings of the 46st Structures, Structural Dynamics, and Materials Conference, Austin, Texas*, (Reston, Virginia), AIAA, April 18 – 21, 2005.

[14] Demasi, L. and Livne, E., "The structural order reduction challenge in the case of geometrically nonlinear joined-wing configurations," in *Proceedings of the 48th Structures, Structural Dynamics, and Materials Conference, Honolulu, Hawaii*, (Reston, Virginia), AIAA, April 23 – 26, 2007. Paper AIAA 2007-2052.

[15] Demasi, L. and Livne, E., "Aeroelastic coupling of geometrically nonlinear structures and linear unsteady aerodynamics: Two formulations," in *Proceedings of the 49th Structures, Structural Dynamics, and Materials Conference, Schaumburg, Illinois*, (Reston, Virginia), AIAA, April 7 – 10, 2008. Paper AIAA 2008-1758.

[16] Demasi, L. and Livne, E., "Contributions to joined-wing aeroelasticity," in *CEAS/AIAA/DGLR International Forum on Aeroelasticity and Structural Dynamics, Seattle, Washington*, June 22 – 24, 2009.

[17] Dreibelbis, B. and Barth, J., "Structural analysis of joint wings," in *Proceedings of Regional Student Conference*, (Baltimore, Maryland), AIAA, April 2003.

[18] Gaonkar, G. H. and Peters, D. A., "Use of multiblade coordinates for helicopter flap-lag stability with dynamic inflow," *Journal of Aircraft*, vol. 1, pp. 112 – 118, February 1980.

[19] Ghorashi, M. and Nitzsche, F., "Nonlinear dynamic response of an accelerating composite rotor blade using perturbations," *Journal of Mechanics of Materials and Structures*, vol. 4, no. 4, pp. 693 – 718, 2009.

[20] Giavotto, V., Borri, M., Mantegazza, P., Ghiringhelli, G., Carmaschi, V., Maffioli, G. C., and Mussi, F., "Anisotropic beam theory and applications," *Computers and Structures*, vol. 16, no. 1-4, pp. 403 – 413, 1983.

[21] Goland, M., "The flutter of a uniform cantilever wing," *Journal of Applied Mechanics*, vol. 12, pp. A197 – A208, December 1945.

[22] Goyal, S., Perkins, N., and Lee, C., "Nonlinear dynamics and loop formation in kirchhoff rods with implications to the mechanics of dna and cables," *Journal of Computational Physics*, vol. 209, pp. 371 – 389, 2005.

[23] Green, N. S., Canfield, R. A., Swenson, E., Yu, W., and Blair, M., "Structural optimization of joined-wing beam model with bend-twist coupling using equivalent static loads," in *Proceedings of the 50th Structures, Structural Dynamics, and Materials Conference, Palm Springs, California*, (Reston, Virginia), AIAA, May 4 – 7, 2009. Paper AIAA-2009-2644.

[24] Hegemier, G. A. and Nair, S., "A nonlinear dynamical theory for heterogeneous, anisotropic, elastic rods," *AIAA Journal*, vol. 15, pp. 8–15, January 1977.

[25] Hodges, D. H., "A mixed variational formulation based on exact intrinsic equations for dynamics of moving beams," *International Journal of Solids and Structures*, vol. 26, no. 11, pp. 1253 – 1273, 1990.

[26] Hodges, D. H., Atilgan, A. R., Fulton, M. V., and Rehfield, L. W., "Free-vibration analysis of composite beams," *Journal of the American Helicopter Society*, vol. 36, no. 3, pp. 36 – 47, 1991.

[27] Hodges, D. H. and Bless, R. R., "Axial instability of rotating rods revisited," *International Journal of Non-Linear Mechanics*, vol. 29, pp. 879 – 887, Nov. 1994.

[28] Hodges, D. H. and Dowell, E. H., "Nonlinear equations of motion for the elastic bending and torsion of twisted nonuniform rotor blades," Technical Note TN D-7818, NASA, 1974.

[29] Hodges, D. H. and Ormiston, R. A., "Stability of elastic bending and torsion of uniform cantilever rotor blades in hover with variable structural coupling," Technical Note TN D-8192, NASA, 1976.

[30] Hodges, D. H. and Rutkowski, M. J., "Free-vibration analysis of rotating beams by a variable-order finite-element method," *AIAA Journal*, vol. 19, pp. 1459 – 1466, Nov. 1981.

[31] Hodges, D. H., "Geometrically-exact, intrinsic theory for dynamics of curved and twisted anisotropic beams," *AIAA Journal*, vol. 41, pp. 1131 – 1137, June 2003.

[32] Hodges, D. H., *Nonlinear Composite Beam Theory*. Reston, Virginia: AIAA, 2006.

[33] Hodges, D. H., "Corrigendum: geometrically-exact, intrinsic theory for dynamics of curved and twisted anisotropic beams," *AIAA Journal*, vol. 47, pp. 1308 – 1309, May 2009.

[34] Hodges, D. H., Ho, J. C., and Yu, W., "The effect of taper on section constants for in-plane deformation of an isotropic strip," *Journal of Mechanics of Materials and Structures*, vol. 3, pp. 425 – 440, March 2008.

[35] Hodges, D. H. and Pierce, G. A., *Introduction to Structural Dynamics and Aeroelasticity*. Cambridge, U.K.: Cambridge University Press, 2002.

[36] Kroo, I. and Smith, S., "Aerodynamic and structural studies of joined-wing aircraft," *Journal of Aircraft*, vol. 28, no. 1, pp. 74–81, 1991.

[37] Lee, D. H. and Chen, P. C., "Nonlinear aeroelastic studies on a joined-wing with wing buckling effects," in *Proceedings of the 45th Structures, Structural Dynamics, and Materials Conference, Palm Springs, California*, (Reston, Virginia), AIAA, April 19 – 22, 2004. Paper AIAA 2004-1944.

[38] Liu, S., Wickert, D. P., and Canfield, R. A., "Fluid-structure transient gust response sensitivity for a nonlinear joined wing model," in *Proceedings of the 51st Structures, Structural Dynamics, and Materials Conference, Orlando, Florida*, (Reston, Virginia), AIAA, April 12 – 15, 2010. Paper AIAA-2010-3118.

[39] Livne, E., "Aeroelasticity of joined-wing airplane configurations: past work and future challenges – a survey," in *Proceedings of the 42nd Structures, Structural Dynamics, and Materials Conference, Seattle, WA*, (Reston, Virginia), AIAA, April 16 – 19, 2001. Paper AIAA 2001-1370.

[40] Lu, C.-L. and Perkins, N., "Nonlinear spatial equilibria and stability of cables under uni-axial torque and thrust," *Journal of Applied Mechanics*, vol. 61, no. 4, pp. 879 – 886, 1994.

[41] Paletta, N., Belardo, M., and Pecora, M., "Load alleviation on a joined wing unmanned aircraft," *Journal of Aircraft*, vol. 47, no. 6, pp. 2005 –2016, 2010.

[42] Paletta, N., Belardo, M., and Pecora, M., "Incremental method for structural analysis of joined-wing aircraft," *Journal of Aircraft*, 2011. To appear.

[43] Patil, M. J., "Nonlinear aeroelastic analysis of joined-wing aircraft," in *Proceedings of the 44th Structures, Structural Dynamics and Materials Conference, Norfolk, Virginia*, (Reston, Virginia), AIAA, April 7 – 10, 2003. Paper AIAA 2003-1487.

[44] Patil, M. J. and Hodges, D. H., "Flight dynamics of highly flexible flying wings," *Journal of Aircraft*, vol. 43, no. 6, pp. 1790–1799, 2006.

[45] Patil, M. J., Hodges, D. H., and Cesnik, C. E. S., "Limit cycle oscillations in high-aspect-ratio wings," in *Proceedings of the 40th Structures, Structural Dynamics and Materials Conference, Saint Louis, Missouri*, pp. 2184 – 2194, April 12 – 15, 1999. AIAA Paper 99-1464.

[46] Patil, M. J. and Hodges, D. H., "Variable-order finite elements for nonlinear, intrinsic, mixed beam equations," in *Proceedings of the 62nd Annual Forum of the American Helicopter Society, Phoenix, Arizona*, American Helicopter Society, May 9 – 11, 2006.

[47] Pereira, P., Almeida, L., Suleman, A., Bond, V., Canfield, R., and Blair, M., "Aeroelastic scaling and optimization of a joined-wing aircraft concept," in *Proceedings of the 48th Structures, Structural Dynamics, and Materials Conference, Honolulu, Hawaii*, (Reston, Virginia), AIAA, April 23 – 26, 2007. Paper AIAA 2004-1944.

[48] Peters, D. A., Karunamoorthy, S., and Cao, W.-M., "Finite state induced flow models; part I: two-dimensional thin airfoil," *Journal of Aircraft*, vol. 32, pp. 313 – 322, Mar.-Apr. 1995.

[49] Peters, D. A. and He, C. J., "Finite state induced flow models. ii - three-dimensional rotor disk," *Journal of Aircraft*, vol. 32, no. 2, pp. 323–333, 1995.

[50] Rasmussen, C., Canfield, R., and Blair, M., "Joined-wing sensor-craft configuration design," *Journal of Aircraft*, vol. 43, no. 5, pp. 161–178, 2006.

[51] Shang, X., Hodges, D. H., and Peters, D. A., "Aeroelastic stability of composite hingeless rotors in hover with finite-state unsteady aerodynamics," *Journal of the American Helicopter Society*, vol. 44, pp. 206 – 221, July 1999.

[52] Simo, J. C. and Vu-Quoc, L., "On the dynamics of flexible beams under large overall motions – the plane case: part II," *Journal of Applied Mechanics*, vol. 53, pp. 855 – 863, December 1986.

[53] Simo, J. C. and Vu-Quoc, L., "On the dynamics in space of rods undergoing large motions – a geometrically exact approach," *Computer Methods in Applied Mechanics and Engineering*, vol. 66, pp. 125–161, 1988. North Holland.

[54] Sotoudeh, Z. and Hodges, D. H., "Nonlinear aeroelastic analysis of joined-wing aircraft with intrinsic equations," in *Proceedings of the 50th Structures, Structural Dynamics, and Materials Conference, Palm Springs, California*, (Reston, Virginia), AIAA, May 4 – 7, 2009. Paper AIAA 2009-2464.

[55] Sotoudeh, Z. and Hodges, D. H., "Modeling beams with various boundary conditions using fully intrinsic equations," in *Proceedings of the 51st Structures, Structural Dynamics, and Materials Conference, Orlando, Florida*, (Reston, Virginia), AIAA, April 12 – 15, 2010.

[56] Sotoudeh, Z. and Hodges, D. H., "Parametric study of joined-wing aircraft geometry," in *Proceedings of the 51st Structures, Structural Dynamics, and Materials Conference, Orlando, Florida*, (Reston, Virginia), AIAA, April 12 – 15, 2010. Paper AIAA-2010-2718.

[57] Sotoudeh, Z. and Hodges, D. H., "Modeling beams with various boundary conditions using fully intrinsic equations," *Journal of Applied Mechanics*, vol. 78, no. 1, 2011. article 031010.

[58] Sotoudeh, Z. and Hodges, D. H., "Stability analysis and dynamic response of rotating blades using fully intrinsic equations," in *Proceedings of the 67th Annual Forum of the American Helicopter Society*, May 2011.

[59] Sotoudeh, Z., Hodges, D. H., and Chang, C.-S., "Validation studies for nonlinear aeroelastic trim and stability of HALE aircraft," in *CEAS/AIAA/DGLR International Forum on Aeroelasticity and Structural Dynamics, Seattle, Washington*, June 22 – 24, 2009.

[60] Sotoudeh, Z., Hodges, D. H., and Chang, C., "Validation studies for aeroelastic trim and stability analysis of highly flexible aircraft," *Journal of Aircraft*, vol. 47, no. 4, pp. 1240 – 1247, 2010.

[61] Tang, D. M. and Dowell, E. H., "Flutter and stall response of a helicopter blade with structural nonlinearity," *Journal of Aircraft*, vol. 29, no. 5, pp. 935–960, 1992.

[62] Weisshaar, T. A. and Lee, D. H., "Aeroelastic tailoring of joined-wing configurations," in *Proceedings of the 43rd Structures, Structural Dynamics, and Materials Conference, Denver, Colorado*, (Reston, Virginia), AIAA, April 22 – 25, 2002. Paper AIAA 2002-1207.

[63] Wolkovitch, J., "The joined wing: an overview," *Journal of Aircraft*, vol. 23, no. 3, pp. 161–178, 1986.

[64] Wright, A. D., Smith, C. E., Thresher, R. W., and Wang, J. L. C., "Vibration modes of centrifugally stiffened beams," *Journal of Applied Mechanics*, vol. 49, pp. 197 – 202, March 1982.

[65] Yu, W., Hodges, D. H., Volovoi, V. V., and Cesnik, C. E. S., "On Timoshenko-like modeling of initially curved and twisted composite beams," *International Journal of Solids and Structures*, vol. 39, no. 19, pp. 5101 – 5121, 2002.

[66] Yuan, K. A. and Friedmann, P. P., "Aeroelasticity and structural optimization of composite helicopter rotor blades with swept tips," Tech. Rep. 4665, NASA, May 1995.

VITA

Zahra Sotoudeh received her Bachelor of Science degree in aerospace engineering in 2004 from Polytechnique de Tehran, Tehran, Iran. She received her Master of Science in Aerospace Engineering in 2006 from Sharif University of Technology, Tehran, Iran. She started her studies at the Georgia Institute of Technology, Atlanta, Georgia, in January 2007. She received a Master of Science in 2009 and a Doctor of Philosophy in August 2011, both in aerospace engineering.